[American Journal of Science, Vol. 301, April/May, 2001, P. 326–358]

SLOW RATES OF ROCK SURFACE EROSION AND SEDIMENT PRODUCTION ACROSS THE NAMIB DESERT AND ESCARPMENT, SOUTHERN AFRICA

PAUL R. BIERMAN* and MARC CAFFEE**

ABSTRACT. Slow erosion has characterized the Namib Desert, the Namibian escarpment, and the adjacent Namibian highlands over the Pleistocene. Paired analyses (n=66) of in-situ-produced ^{10}Be and ^{26}Al in quartz-bearing samples of bedrock primarily from inselbergs, of sediment from dry river and stream channels, and of clasts from desert surfaces reveal large inventories of these cosmogenic nuclides indicating significant landscape stability over at least the past million years.

Bedrock samples (n = 47) collected in three transects from the coast, across the escarpment, and into the highlands, show no spatial pattern in elevation-normalized nuclide abundance despite a difference in mean annual precipitation (MAP) between sample sites at the coast (MAP <25 mm yr^{-1}) and those in the highlands (MAP >400 mm yr^{-1}). Average model erosion rates inland of the escarpment (3.2 ± 1.5, n = 9) are indistinguishable from average rates seaward of the escarpment (3.6 ± 1.9, n = 38) indicating that rock on the pedimented coastal plain is eroding at the same rate as rock in the highlands. Sediment samples (n = 3) from small streams suggest that the landscape as a whole is eroding more rapidly than the bedrock outcrops and that a basin in the steep escarpment zone is eroding several times faster (16 m my^{-1}) than either a basin in the highlands (5 m my^{-1}) or a basin in the coastal plain (8 m my^{-1}). Data from large rivers (n = 4) constrain erosion rates, averaged over 10^5 yrs and 10^4 to 10^5 km^2, between 3 and 9 m my^{-1}. Small quartz clasts (n = 12) collected from four desert surfaces record extraordinarily long, variable, and in some cases complex exposure histories. Simple ^{10}Be model ages are as high as 1.8 my; some minimum total histories, considering both ^{10}Be and ^{26}Al and including both burial and exposure, exceed 2.7 my. As a group, the Namibian cosmogenic data do not support the model of significant and on-going escarpment retreat.

The similarity of erosion rates calculated from ^{10}Be analysis of fluvial sediments and longer-term (10^7 yr), average mass removal rates estimated by others using fission track analysis of rock suggests that Namibian erosion rates have reached a steady state and are changing little over time. At outcrop scales, the concordance of ^{10}Be and ^{26}Al in most bedrock samples suggests that the model of steady, uniform bedrock erosion is valid; there is no indication of intermittent burial, shedding of thick rock slabs, or stripping of previous cover. At an intermediate scale, a transect of bedrock samples north of Gobabeb demonstrates that the northern boundary of the massive Namib Sand Sea has been steady and unshifting. Similarly low cosmogenically estimated erosion rates across west and central Namibia suggest that the landscape is in geomorphic steady state, its overall appearance changing only slowly through time.

INTRODUCTION

Namibia, with its passive margin setting, relative tectonic stability, and arid climate is a classic location to investigate the proposition that landscapes achieve steady state in terms of both denudation rates and geomorphic appearance over time (fig. 1). Much of southern Africa, including Namibia, is dominated by a wide coastal plain pediment, a steep escarpment zone, and rolling highlands. These landscape elements are central to the qualitative paradigm of rapid, parallel, and on-going escarpment retreat (pediplanation) as the means by which planation surfaces, especially expansive coastal

*Department of Geology and School of Natural Resources, University of Vermont, Burlington, Vermont 05405-0122

**Center for Accelerator Mass Spectrometry, Lawrence Livermore Laboratory, Livermore, California 94550

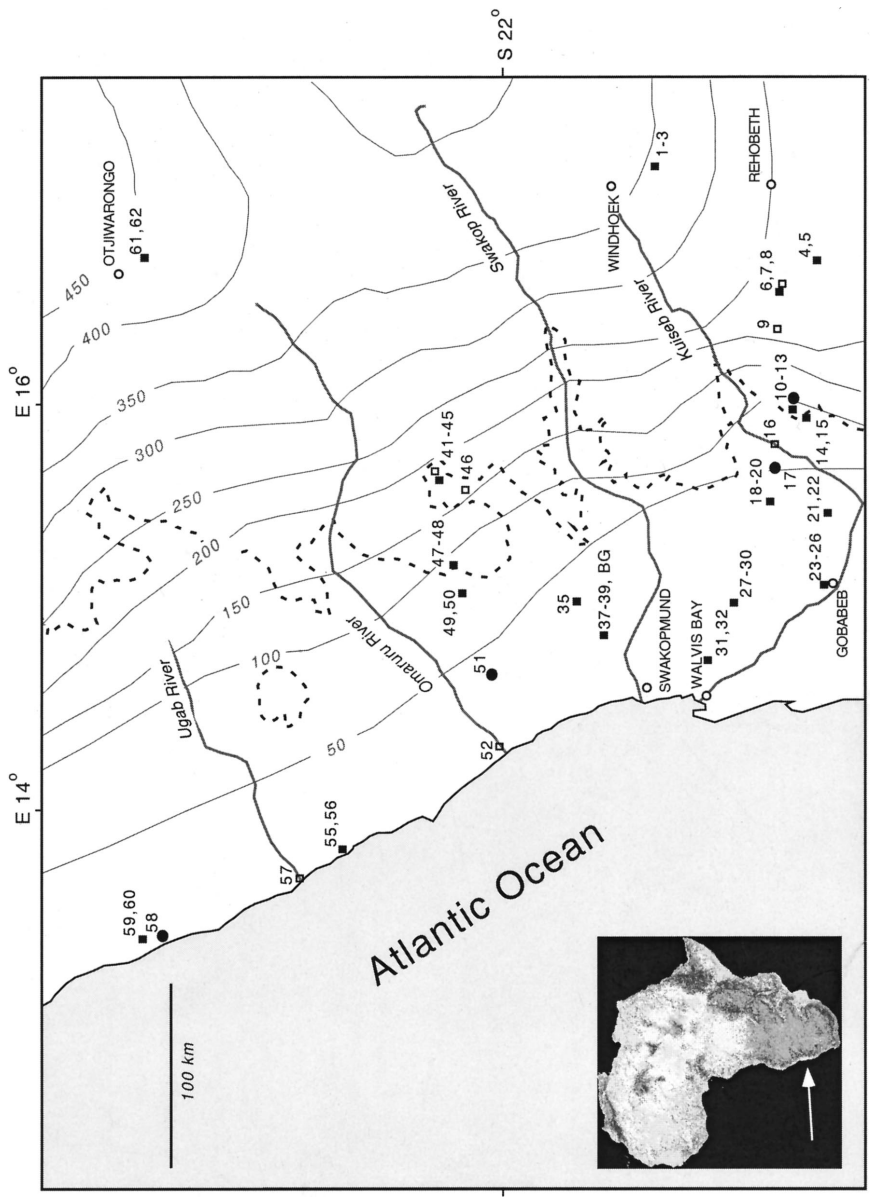

Fig. 1. Location of cosmogenic sample sites (NAM) indicated by number. Filled squares are bedrock samples; filled circles are clast samples; open squares are sediment samples; open circles are cities. Dashed line is 1000 m contour which approximately defines the coastal plain/escarpment junction. Primary channel of major ephemeral rivers shown by thick gray lines. Thin gray lines are isohyets of mean annual precipitation in mm yr^{-1}, adapted from Jacobsen, Jacobsen, and Seely (1995). Inset is digital elevation model of southern Africa with arrow showing study area including escarpment, coastal plain, and highlands. Shading represents elevation; darker is higher.

plain pediments, are formed (King, 1953, 1957; 1967; Partridge and Maud, 1987). More recently, numerical models have been used to simulate landscape processes of escarpment retreat and pediment formation (Gilchrist and others, 1994; Gilchrist and Summerfield, 1990; Kooi and Beaumont, 1994; van der Beek and others, 1998; Tucker and Slingerland, 1994). These models rely upon empirical calibration of erosion rates over time.

Recent advances in geochronology (analysis of cosmogenic isotopes produced *in situ* and fission track analysis) provide a different and novel means by which to understand landscape change quantitatively. The analysis of cosmogenic nuclides, those formed by nuclear interaction of cosmic radiation with common rock-forming minerals, allows estimation of near-surface residence times and thus erosion rates for exposed crustal materials over the 10^3 to 10^6 yr time frame (Bierman, 1994; Cerling and Craig, 1994; Davis and Schaeffer, 1955; Lal, 1988; Lal and Peters, 1967). In contrast, fission track analysis provides mass removal data on a longer time scale, 10^6 to 10^8 yr, Cosmogenic isotope and fission track analysis are complementary tools capable of estimating the location and magnitude of mass removal from Earth's surface over differing time and length scales.

This paper describes the Pleistocene erosional history of Namibia based on paired nuclide (^{10}Be and ^{26}Al) analyses of 66 quartz-bearing samples collected over a wide area of west-central Namibia (tables 1-5). Our work builds upon the work done by Cockburn, Seidl, and Summerfield (1999) and Cockburn and others (2000) in Namibia by greatly expanding the number, type, and spatial coverage of cosmogenic nuclide analyses. We compare our new data to existing fission track measurements (Brown and others, 2000; Cockburn and others, 2000; Gallagher and Brown, 1997, 1999) and use the combination to evaluate existing paradigms of landscape behavior.

SETTING

Three elements dominate the Namibian landscape of southwestern Africa: a major, coast-parallel escarpment zone, the Namib Desert, and the highlands landward of the escarpment (fig. 1, inset). The escarpment rises 500 to 1000 m from the edge of the Namib Desert to the highlands (fig. 2). In some places the escarpment is quite distinct; in other places it is dissected, and the transition from the coastal plain desert to the more humid highlands is a gradual one. Above the escarpment are rolling highlands where precipitation is sufficient to support extensive vegetation and the development of at least minimal colluvium on hillslopes (figs. 1 and 3). Where coarse crystalline rocks crop out, inselbergs are common both above and below the escarpment (Ollier, 1978).

The escarpment initiated during the breakup of Africa and South America, 135 my (Brown and others, 2000; Partridge and Maud, 1987; Ward and Corbett, 1990). Some suggest that since then the main escarpment as well as other smaller escarpments resulting from base level changes have retreated steadily (King, 1967) and in a parallel fashion (Penck, 1924) to their current position, on avg 150 km from the coast in central Namibia. Others suggest initial or delayed but still rapid denudation of the coastal plane with or without subsequent slow escarpment retreat (Partridge and Maud, 1987; Brown and others, 2000; Cockburn and others, 2000; Gallagher and Brown, 1999; Summerfield and others, 1997; Ward and Corbett, 1990; van der Beek and others, 1998).

The former scenario implies an average, on-going escarpment retreat rate of about a kilometer every million years. The latter scenario implies a current retreat rate of meters to tens of meters per million years. The retreat of the escarpment left behind the beveled coastal plain, also referred to as the Namibian Unconformity Surface (Ollier, 1977), upon which a thin and discontinuous cover of Tertiary sediments can be found. Offshore sediment volume data, summarized by Ward and Corbett (1990),

suggest rapid escarpment retreat and extensive sediment generation in the Cretaceous during which time the coastal plain formed. By the Tertiary, sedimentation rates off shore dropped significantly (Ward and Corbett, 1990).

The Namib Desert extends across this coastal plain from the base of the escarpment (approx 1000 m above sealevel, fig. 1) to the Southern Atlantic Ocean. The desert is generally a low relief surface where bedrock is rarely far below the discontinuous cover of alluvium and colluvium. There is no deep regolith (Selby, 1977). The Namib Desert is punctuated by inselbergs (fig. 4), isolated outcroppings of rock commonly surrounded by pediments, gently dipping bare or nearly bare bedrock surfaces (Selby, 1977, 1982a,b; Cockburn, Seidl, and Summerfield, 1999; Ollier, 1978). The origin of these inselbergs is uncertain; some argue for stripping of deep regolith in Africa and elsewhere (Twidale, 1978; Oberlander, 1972); others argue that these are inselbergs of position sequentially exposed by the retreating escarpment (King, 1966; Selby, 1977; Thomas, 1978).

Exposed rock surfaces in Namibia are usually weathered; mass is often lost either by granular disintegration or by the exfoliation of thin (centimeter-scale) sheets (fig. 3). Salty efflorescences are particularly common near the coast suggesting that salt-induced weathering is important in the breakdown of rock in this zone (Goudie, 1972). In particularly windy locations, both rock outcrops and clasts on desert surfaces are well ventifacted; the sand blasted rock is fresh and unweathered.

Extensive low-relief gravel surfaces occur within and seaward of the escarpment zone (Ward, 1987; Ward and Corbett, 1990). These surfaces extend for kilometers and are typically covered by rock clasts, many of which are composed of quartz or chert (fig. 5). The clasts are competent, unweathered, and polished; the frequency and style of polish suggest the polishing is done by wind. Most of the surfaces have little if any vegetation present. These appear to be deflational surfaces with gravel and sand lags overlying carbonate-cemented material (Goudie, 1972). Most of the gravels we sampled are probably part of the Miocene Karpfenkliff formation or one of its equivalents to the north (Ward, 1987). The origin of the gravel sampled at NAM-58 is uncertain; it may be the northern equivalent of the fluvio-marine, Miocene Roikoop gravels described farther south up to an elevation of 90 m asl and reflecting a Miocene sealevel rise (Ward, 1987).

The extensive Miocene gravels have been interpreted to suggest a more moisture-effective hydrologic regime, at least in the highlands, at the time of their deposition. The thick and extensive carbonate cement is a later Miocene addition, termed the Kamberg Calcrete (Ward, 1987). The continued existence of the calcrete reflects increasing Namibian aridity since the Miocene. The excellent preservation of the carbonate implies that aridity has been maintained, in general, to the present day (Ward and Corbett, 1990). The gravels and calcrete represent the last widespread deposition on the piedmont before deep incision into the coastal plain by the escarpment-crossing rivers. The incision and the consequent preservation of paleo surfaces have been attributed to late Tertiary/Quaternary epirogeny (Partridge and Maud, 1987; Ward, 1987; Ward and Corbet, 1990).

Namibia is a dry landscape and the Namib desert is particularly so. Subtropical easterly winds move over the African continent losing their moisture before descending the escarpment and drying further. The south Atlantic anticyclone, the cold Benguela current, and consequent coastal upwelling offshore of Namibia ensure little precipitation reaches the coast. Mean annual precipitation is <25 mm on the coast, 50 to 200 mm at the base of the escarpment, and 200 to 450 mm on the highlands above the escarpment (fig. 1 and Jacobsen, Jacobsen, and Seely, 1995). Fog drip is an important moisture source on the coastal plain (Jacobsen, Jacobsen, and Seely, 1995). All rivers and streams originating in Namibia are ephemeral; the only perennial rivers

TABLE 1

A. Location and description of cosmogenic nuclide samples from Namibia

Sample	GPS Latitude (UTM)[1]	GPS Longitude (UTM)[1]	type[2]	Lithology[3]	Ranch[4]	Site Name
NAM-01	33K0718259	7484479	in	granite	Aris 29	Falkenstein
NAM-02	33K0718257	7484467	in	granite	Aris 29	Falkenstein
NAM-03	33K0718216	7484424	in	granite	Aris 29	Falkenstein
NAM-04	33K0674162	7401384	in	quartztite	Barnadespan 322	Barnadespan
NAM-05	33K0674171	7401453	in	quartztite	Barnadespan 322	Barnadespan
NAM-06	33K0651258	7423051	in	granite	Weissenfels 22	Weissenfels
NAM-07	33K0651236	7423027	in	granite	Weissenfels 22	Weissenfels
NAM-08	33K0648196	7420624	sed	sediment	Weissenfels 22	Weissenfels
NAM-09	33K0633006	7428527	sed	sediment	Djab 26	escarpment
NAM-10	33K0597065	7416125	in	gneiss	Berghof 222	Berghof
NAM-11	33K0597053	7416105	in	gneiss	Berghof 222	Berghof
NAM-12	33K0597053	7416105	in	quartz	Berghof 222	Berghof
NAM-13	33K0599394	7415840	cl	quartz	Berghof 222	Berghof
NAM-14	33K0591631	7411757	in	granite	Rostock 393	Sandsteenberg
NAM-15	33K0592366	7411666	in	gneiss	Rostock 393	Sandsteenberg
NAM-16	33K0579139	7422652	sed	sediment	106	Kuiseb Canyon
NAM-17	33K0567785	7419816	cl	quartz	N.A.	Aruvlie Signpost
NAM-18	33K0544553	7425098	in	pegmatite	N.A.	pegmatite
NAM-19	33K0544562	7425191	in	quartz	N.A.	pegmatite
NAM-20	33K0544562	7425191	in	quartz	N.A.	pegmatite
NAM-21	33K0537494	7404255	in	granite	N.A.	east of Mirabib
NAM-22	33K0537603	7404178	in	granite	N.A.	east of Mirabib
NAM-23	33K0504595	7394912	oc	granite	N.A.	Gobabeb
NAM-24	33K0504793	7395337	oc	granite	N.A.	Gobabeb
NAM-25	33K0504890	7396186	oc	granite	N.A.	Gobabeb
NAM-26	33K0504820	7396423	oc	granite	N.A.	Gobabeb
NAM-27	33K0498813	7450259	in	granite	N.A.	Vogelfederberg
NAM-28	33K0498789	7450312	in	granite	N.A.	Vogelfederberg
NAM-29	33K0498800	7450316	in	granite	N.A.	Vogelfederberg
NAM-30	33K0498832	7450376	in	granite	N.A.	Vogelfederberg
NAM-31	33K0464187	7456606	in	granite	N.A.	Roikop
NAM-32	33K0464550	7457364	in	granite	N.A.	Roikop
NAM-35	33K0500781	7522506	in	gneiss	N.A.	Arandisberg
NAM-37	33K0482948	7508019	in	gneiss	N.A.	Rossinberg
NAM-38	33K0482948	7508019	in	gneiss	N.A.	Rossinberg
NAM-39	33K0482876	7507947	in	gneiss	N.A.	Rossinberg
NAM-41	33K0566269	7589087	in	granite	Ameib 60	Phillips Cave
NAM-42	33K0566290	7589123	in	granite	Ameib 60	Phillips Cave
NAM-43	33K0566102	7589648	sed	sediment	Ameib 60	Phillips Cave
NAM-44	33K0567580	7591185	in	granite	Ameib 60	Bulls Party
NAM-45	33K0567571	7591137	in	granite	Ameib 60	Bulls Party
NAM-46	33K0559300	7576359	sed	sediment	Goabib 63	Kahn River
NAM-47	33K0519417	7584769	in	granite	Gross Spitzkoppe 71	Gross Spitzkoppe
NAM-48	33K0519424	7584775	in	granite	Gross Spitzkoppe 71	Gross Spitzkoppe
NAM-49	33K0502794	7579279	in	granite	Hoppverloor 88	African Granite Mine
NAM-50	33K0502794	7579279	in	granite	Hoppverloor 88	African Granite Mine
NAM-51	33K0468308	7569938	cl	quartz	Aris 29	Henties Surface
NAM-52	33K0424543	7557504	sed	sediment	Aris 29	Omaruru River
NAM-55	33K0373427	7639080	oc	quartz	N.A.	Bandombaai
NAM-56	33K0373427	7639080	oc	quartz	N.A.	Bandombaai
NAM-57	33K0361472	7659077	sed	sediment	N.A.	Ugab River
NAM-58	33K0327921	7728208	cl	quartz	N.A.	Soutpan surface
NAM-59	33K0323717	7740123	in	granite gneiss	N.A.	Palgrave
NAM-60	33K0323690	7740117	in	granite gneiss	N.A.	Palgrave
NAM-61	33K0676451	7730104	in	granite	Otjiwarongo Town Lands S.	Otjiwarongo
NAM-62	33K0676451	7730104	in	granite	Otjiwarongo Town Lands S.	Otjiwarongo
NAMBG1A	33K0483278	7508203	oc	gneiss	N.A.	Rossinberg
NAMBG1B	33K0483278	7508203	oc	gneiss	N.A.	Rossinberg

N.A. = Not available; N.D. = no data; [1] measured with Garmin 12; referenced to WGS 84; [2] in = inselberg, sed = sediment sample, cl = pavement clasts, oc = outcrop; [3] taken from Geologic map of Southwest Africa, Miller and Schalk (1980); [4] as identified on South African 1:250,000 topographic maps; [5] determined by GPS; [6] determined from 1:250,000 maps; [7] determined from 1:50,000 maps.

TABLE 1

B. Location and description of cosmogenic nuclide samples from Namibia

1:250,000 Mapsheet	1:50,000 Mapsheet	Elevation[5] (m)	Elevation[6] (m)	Elevation[7] (m)	Sample
Windhoek 2216	N.A.	2003	2025	N.D	NAM-01
Windhoek 2216	N.A.	1974	2025	N.D	NAM-02
Windhoek 2216	N.A.	1972	2025	N.D	NAM-03
Rehoboth 2316	Gollschoru 2316BC	1709	1675	1678	NAM-04
Rehoboth 2316	Gollschoru 2316BC	1673	1675	1678	NAM-05
Rehoboth 2316	Hornkrantz 2316AB	1938	1836	1836	NAM-06
Rehoboth 2316	Hornkrantz 2316AB	1880	1836	1836	NAM-07
Rehoboth 2316	Hornkrantz 2316AB	1783	1775	1750	NAM-08
Rehoboth 2316	Hakos 2316AB	1455	1425	1390	NAM-09
Kuiseb 2314	Rostok 2315BD	1073	1098	1083	NAM-10
Kuiseb 2314	Rostok 2315BD	1120	1098	1083	NAM-11
Kuiseb 2314	Rostok 2315BD	1120	1098	1083	NAM-12
Kuiseb 2314	Rostok 2315BD	1072	1025	1057	NAM-13
Kuiseb 2314	Rostok 2315BD	1015	1025	1000	NAM-14
Kuiseb 2314	Rostok 2315BD	983	1025	980	NAM-15
Kuiseb 2314	Rostok 2315BD	N.D	775	748	NAM-16
Kuiseb 2314	N.A.	1011	925	N.D	NAM-17
Kuiseb 2314	Sebrapan 2315AD	869	825	867	NAM-18
Kuiseb 2314	Sebrapan 2315AD	866	825	867	NAM-19
Kuiseb 2314	Sebrapan 2315AD	866	825	867	NAM-20
Kuiseb 2314	Sebrapan 2315AD	800	791	782	NAM-21
Kuiseb 2314	Sebrapan 2315AD	769	791	782	NAM-22
Kuiseb 2314	Gobabeb 231CA	434	435	401	NAM-23
Kuiseb 2314	Gobabeb 231CA	451	435	410	NAM-24
Kuiseb 2314	Gobabeb 231CA	447	435	420	NAM-25
Kuiseb 2314	Gobabeb 231CA	565	435	420	NAM-26
Kuiseb 2314	2314BB	570	525	518	NAM-27
Kuiseb 2314	2314BB	546	525	518	NAM-28
Kuiseb 2314	2314BB	528	525	505	NAM-29
Kuiseb 2314	2314BB	546	525	505	NAM-30
Walvis Baai 2214	N.A.	78	100	N.D	NAM-31
Walvis Baai 2214	N.A.	57	75	N.D	NAM-32
Walvis Baai 2214	Trekkopje 2215AC	733	675	650	NAM-35
Walvis Baai 2214	Goan 2214DB	459	500	510	NAM-37
Walvis Baai 2214	Goan 2214DB	459	500	510	NAM-38
Walvis Baai 2214	Goan 2214DB	555	500	510	NAM-39
Omaruru 2114	Usakos 2115DC	1220	1175	1190	NAM-41
Omaruru 2114	Usakos 2115DC	1223	1175	1190	NAM-42
Omaruru 2114	Usakos 2115DC	NA	1075	1070	NAM-43
Omaruru 2114	Usakos 2115DC	1225	1225	1210	NAM-44
Omaruru 2114	Usakos 2115DC	1199	1225	1210	NAM-45
Omaruru 2114	Usakos 2115DC	885	925	910	NAM-46
Omaruru 2114	Spitzkoppen 2115CC	1163	1175	1150	NAM-47
Omaruru 2114	Spitzkoppen 2115CC	1140	1175	1150	NAM-48
Omaruru 2114	Spitzkoppen 2115CC	913	950	956	NAM-49
Omaruru 2114	Spitzkoppen 2115CC	913	950	956	NAM-50
Omaruru 2114	N.A.	508	450	N.D	NAM-51
Walvis Baai 2214	N.A.	-23	75	N.D	NAM-52
Kaap Kruis 2013	Ugab Salt 2113DD	0	25	10	NAM-55
Kaap Kruis 2013	Ugab Salt 2113DD	0	25	10	NAM-56
Kaap Kruis 2013	N.A.	27	25	N.D	NAM-57
Kaap Kruis 2013	N.A.	-30	25	N.D	NAM-58
Kaap Kruis 2013	Torrabaai 2013AC	142	75	62	NAM-59
Kaap Kruis 2013	Torrabaai 2013AC	100	75	62	NAM-60
Otjiwarongo 2016	Parasis 2016DA	1549	1525	1582	NAM-61
Otjiwarongo 2017	Parasis 2016DA	1549	1525	1582	NAM-62
Walvis Baai 2214	Goanikontes 2214DB	428	425	430	NAMBG1A
Walvis Baai 2214	Goanikontes 2214DB	428	425	430	NAMBG1B

TABLE 2

Cosmogenic nuclide data, samples from Namibia

Sample	^{10}Be measured[1] (10^6 atom g^{-1})	^{26}Al measured[1] (10^6 atom g^{-1})	^{10}Be/^{26}Al	^{10}Be (SL, >60°)[2] (10^6 atom g^{-1})	^{26}Al (SL, >60°)[2] (10^6 atom g^{-1})	Correction for sample thickness[3]
NAM-01	4.77 ± 0.19	26.88 ± 1.23	5.64 ± 0.34	1.54 ± 0.06	8.69 ± 0.40	1.02
NAM-02	4.11 ± 0.10	22.80 ± 0.98	5.54 ± 0.28	1.34 ± 0.03	7.43 ± 0.32	1.03
NAM-03	3.21 ± 0.10	18.22 ± 0.85	5.67 ± 0.32	1.04 ± 0.03	5.89 ± 0.27	1.02
NAM-04	3.02 ± 0.13	18.12 ± 0.87	6.00 ± 0.39	1.22 ± 0.05	7.31 ± 0.35	1.02
NAM-05	1.93 ± 0.05	11.31 ± 0.54	5.85 ± 0.32	0.77 ± 0.02	4.52 ± 0.22	1.02
NAM-06	1.58 ± 0.05	10.01 ± 0.46	6.36 ± 0.36	0.57 ± 0.02	3.63 ± 0.17	1.02
NAM-07	5.50 ± 0.15	31.36 ± 1.39	5.70 ± 0.30	2.03 ± 0.06	11.56 ± 0.51	1.04
NAM-07x[4]	5.45 ± 0.18	31.86 ± 1.50	5.84 ± 0.34	2.01 ± 0.07	11.74 ± 0.55	1.04
NAM-08	1.84 ± 0.05	9.88 ± 0.53	5.36 ± 0.32	0.69 ± 0.02	3.71 ± 0.20	1.00
NAM-09	0.57 ± 0.02	2.96 ± 0.16	5.21 ± 0.33	0.27 ± 0.01	1.43 ± 0.08	1.00
NAM-10	1.25 ± 0.04	7.79 ± 0.38	6.21 ± 0.35	0.77 ± 0.02	4.80 ± 0.24	1.02
NAM-11	1.33 ± 0.04	8.16 ± 0.44	6.11 ± 0.38	0.83 ± 0.02	5.09 ± 0.28	1.03
NAM-12	1.04 ± 0.03	5.99 ± 0.29	5.74 ± 0.32	0.65 ± 0.02	3.73 ± 0.18	1.03
NAM-13A	2.33 ± 0.05	11.71 ± 0.59	5.02 ± 0.28	1.51 ± 0.03	7.57 ± 0.38	1.03
NAM-13B	2.43 ± 0.06	12.44 ± 0.57	5.12 ± 0.26	1.57 ± 0.04	8.05 ± 0.37	1.03
NAM-13C	2.59 ± 0.06	13.43 ± 0.61	5.19 ± 0.26	1.70 ± 0.04	8.82 ± 0.40	1.04
NAM-14	1.67 ± 0.05	9.70 ± 0.44	5.82 ± 0.32	1.09 ± 0.03	6.32 ± 0.29	1.02
NAM-15	2.00 ± 0.06	10.97 ± 0.50	5.49 ± 0.30	1.33 ± 0.04	7.32 ± 0.34	1.02
NAM-16	0.83 ± 0.02	4.36 ± 0.23	5.22 ± 0.32	0.65 ± 0.02	3.38 ± 0.18	1.00
NAM-17B	9.75 ± 0.22	31.57 ± 1.41	3.24 ± 0.16	6.83 ± 0.15	22.13 ± 0.99	1.03
NAM-17C	8.21 ± 0.18	29.45 ± 1.34	3.59 ± 0.18	5.71 ± 0.13	20.50 ± 0.93	1.02
NAM-17D	10.49 ± 0.23	32.62 ± 1.46	3.11 ± 0.16	7.36 ± 0.16	22.87 ± 1.03	1.03
NAM-18	1.40 ± 0.04	7.66 ± 0.41	5.46 ± 0.34	1.03 ± 0.03	5.60 ± 0.30	1.03
NAM-19	1.81 ± 0.07	10.98 ± 0.61	6.08 ± 0.41	1.33 ± 0.05	8.09 ± 0.45	1.04
NAM-20	1.93 ± 0.10	11.76 ± 0.69	6.11 ± 0.49	1.42 ± 0.08	8.66 ± 0.51	1.04
NAM-21	1.46 ± 0.05	7.93 ± 0.36	5.45 ± 0.32	1.11 ± 0.04	6.02 ± 0.28	1.01
NAM-22	1.10 ± 0.03	6.48 ± 0.31	5.88 ± 0.33	0.84 ± 0.02	4.96 ± 0.24	1.02
NAM-23	1.78 ± 0.06	9.70 ± 0.54	5.45 ± 0.35	1.80 ± 0.06	9.81 ± 0.55	1.01
NAM-24	1.96 ± 0.06	10.31 ± 0.55	5.25 ± 0.32	1.98 ± 0.06	10.41 ± 0.55	1.01
NAM-25	1.71 ± 0.07	9.25 ± 0.45	5.42 ± 0.35	1.76 ± 0.07	9.54 ± 0.46	1.04
NAM-26	1.47 ± 0.04	8.20 ± 0.40	5.59 ± 0.31	1.47 ± 0.04	8.22 ± 0.40	1.01
NAM-27	0.52 ± 0.02	3.03 ± 0.15	5.80 ± 0.35	0.49 ± 0.02	2.85 ± 0.14	1.01
NAM-28	0.59 ± 0.02	3.59 ± 0.18	6.05 ± 0.35	0.56 ± 0.02	3.36 ± 0.17	1.01

NAM-29	0.70 ± 0.02	3.99 ± 0.18	5.68 ± 0.31	0.68 ± 0.02	3.84 ± 0.18	1.02
NAM-30	0.54 ± 0.02	3.11 ± 0.17	5.75 ± 0.36	0.51 ± 0.02	2.94 ± 0.16	1.01
NAM-31	0.69 ± 0.02	4.40 ± 0.27	6.36 ± 0.44	0.89 ± 0.03	5.66 ± 0.35	1.00
NAM-32	0.36 ± 0.02	2.16 ± 0.13	5.95 ± 0.46	0.47 ± 0.02	2.83 ± 0.17	1.00
NAM-35	1.16 ± 0.03	6.40 ± 0.29	5.51 ± 0.30	1.02 ± 0.03	5.62 ± 0.26	1.03
NAM-37	1.08 ± 0.04	5.96 ± 0.29	5.55 ± 0.33	1.03 ± 0.03	5.69 ± 0.28	1.01
NAM-38	0.85 ± 0.02	4.97 ± 0.24	5.83 ± 0.33	0.81 ± 0.02	4.75 ± 0.23	1.01
NAM-39	0.87 ± 0.03	5.00 ± 0.30	5.78 ± 0.39	0.82 ± 0.03	4.76 ± 0.29	1.01
NAM-41	1.65 ± 0.05	9.39 ± 0.44	5.69 ± 0.32	1.00 ± 0.03	5.69 ± 0.27	1.05
NAM-42	0.92 ± 0.03	5.69 ± 0.27	6.20 ± 0.35	0.54 ± 0.02	3.34 ± 0.16	1.02
NAM-43	0.72 ± 0.02	4.06 ± 0.21	5.65 ± 0.34	0.45 ± 0.01	2.57 ± 0.13	1.00
NAM-44	4.60 ± 0.19	24.13 ± 1.28	5.24 ± 0.35	2.69 ± 0.11	14.08 ± 0.75	1.02
NAM-45	4.21 ± 0.19	22.99 ± 1.32	5.46 ± 0.40	2.42 ± 0.11	13.20 ± 0.76	1.01
NAM-46	0.95 ± 0.03	5.25 ± 0.24	5.50 ± 0.30	0.68 ± 0.02	3.72 ± 0.17	1.00
NAM-47	1.07 ± 0.03	7.60 ± 0.46	7.11 ± 0.47	0.64 ± 0.02	4.56 ± 0.27	1.01
NAM-48	1.53 ± 0.04	8.55 ± 0.46	5.59 ± 0.34	0.97 ± 0.03	5.42 ± 0.29	1.07
NAM-49	2.88 ± 0.08	16.52 ± 0.89	5.73 ± 0.35	2.08 ± 0.06	11.90 ± 0.64	1.05
NAM-50	0.69 ± 0.02	3.75 ± 0.17	5.40 ± 0.29	0.49 ± 0.01	2.66 ± 0.12	1.03
NAM-51-A	1.13 ± 0.04	6.67 ± 0.33	5.93 ± 0.35	1.16 ± 0.04	6.88 ± 0.34	1.03
NAM-51-C	6.13 ± 0.17	21.75 ± 1.00	3.55 ± 0.19	6.29 ± 0.17	22.32 ± 1.02	1.02
NAM-51-F	4.69 ± 0.17	12.92 ± 0.72	2.75 ± 0.18	4.92 ± 0.18	13.52 ± 0.76	1.04
NAM-52	2.95 ± 0.08	15.47 ± 0.67	5.25 ± 0.27	3.92 ± 0.11	20.59 ± 0.90	1.00
NAM-55	1.89 ± 0.05	9.57 ± 0.51	5.06 ± 0.31	2.73 ± 0.08	13.81 ± 0.73	1.02
NAM-56	1.72 ± 0.05	9.00 ± 0.48	5.22 ± 0.31	2.53 ± 0.07	13.20 ± 0.70	1.03
NAM-57	0.81 ± 0.03	4.68 ± 0.28	5.75 ± 0.40	1.15 ± 0.04	6.60 ± 0.39	1.00
NAM-58A	2.71 ± 0.10	10.44 ± 1.16	3.86 ± 0.45	3.96 ± 0.15	15.26 ± 1.70	1.02
NAM-58C	1.21 ± 0.04	5.20 ± 0.37	4.30 ± 0.34	1.78 ± 0.06	7.67 ± 0.55	1.03
NAM-58D	2.28 ± 0.06	10.92 ± 0.55	4.80 ± 0.28	3.31 ± 0.09	15.88 ± 0.80	1.02
NAM-59	1.49 ± 0.04	8.05 ± 0.35	5.39 ± 0.27	2.12 ± 0.06	11.43 ± 0.49	1.02
NAM-60	1.00 ± 0.03	5.59 ± 0.25	5.57 ± 0.29	1.43 ± 0.04	7.96 ± 0.35	1.02
NAM-61	3.32 ± 0.10	18.58 ± 0.80	5.59 ± 0.29	1.51 ± 0.05	8.46 ± 0.36	1.02
NAM-62	1.85 ± 0.05	10.45 ± 0.46	5.66 ± 0.29	0.83 ± 0.02	4.72 ± 0.21	1.01
NAMBG1A	0.89 ± 0.02	4.71 ± 0.21	5.28 ± 0.27	0.90 ± 0.02	4.74 ± 0.21	1.02
NAMBG1B	1.14 ± 0.03	5.99 ± 0.27	5.27 ± 0.27	1.14 ± 0.03	6.02 ± 0.27	1.02

[1] Normalized to LLNL standards prepared by K. Nishiizumi and including blank corrections; error is counting statistics with uncertainty in carrier concentration (Be, 2%) and ICP data (Al, 4%) added quadradically; [2] normalized to sealevel and high latitude using data of Lal (1991) including only spallation production and elevation and latitude of sample site; [3] normalized to surface using attenuation coefficient of 165 g cm^{-2}; [4] replicate sample.

TABLE 3

Interpretation of cosmogenic nuclide data from Namibian bedrock samples

Sample	minimum limiting ^{10}Be model age (kyr)[1]	minimum limiting ^{26}Al model age (kyr)[1]	maximum limiting ^{10}Be model ε (m Myr^{-1})[2]	maximum limiting ^{26}Al model ε (m Myr^{-1})[2]	Type[3]
NAM-01	272 ± 59	269 ± 63	2.1 ± 0.5	2.0 ± 0.6	in
NAM-02	235 ± 50	225 ± 52	2.5 ± 0.6	2.4 ± 0.7	in
NAM-03	180 ± 38	174 ± 39	3.3 ± 0.8	3.2 ± 0.8	in
NAM-04	212 ± 46	221 ± 51	2.7 ± 0.7	2.5 ± 0.7	in
NAM-05	132 ± 28	131 ± 29	4.5 ± 1.0	4.4 ± 1.1	in
NAM-06	97 ± 20	104 ± 22	6.2 ± 1.4	5.6 ± 1.3	in
NAM-07	362 ± 80	384 ± 96	1.6 ± 0.4	1.3 ± 0.4	in
NAM-07X	366 ± 80	376 ± 93	1.5 ± 0.4	1.3 ± 0.4	in
NAM-10	132 ± 27	140 ± 31	4.5 ± 1.0	4.1 ± 1.0	in
NAM-11	143 ± 30	149 ± 33	4.1 ± 0.9	3.8 ± 1.0	in
NAM-12	111 ± 23	107 ± 23	5.4 ± 1.2	5.4 ± 1.3	in
NAM-14	188 ± 40	188 ± 42	3.1 ± 0.7	3.0 ± 0.8	in
NAM-15	233 ± 50	221 ± 51	2.5 ± 0.6	2.5 ± 0.7	in
NAM-18	177 ± 37	165 ± 37	3.3 ± 0.8	3.4 ± 0.9	in
NAM-19	233 ± 50	248 ± 58	2.5 ± 0.6	2.2 ± 0.6	in
NAM-20	249 ± 55	268 ± 64	2.3 ± 0.6	2.0 ± 0.6	in
NAM-21	192 ± 41	179 ± 40	3.0 ± 0.7	3.1 ± 0.8	in
NAM-22	145 ± 30	145 ± 32	4.1 ± 0.9	3.9 ± 1.0	in
NAM-23	321 ± 70	310 ± 75	1.8 ± 0.4	1.7 ± 0.5	oc
NAM-24	356 ± 78	332 ± 81	1.6 ± 0.4	1.6 ± 0.5	oc
NAM-25	314 ± 69	300 ± 72	1.8 ± 0.5	1.8 ± 0.5	oc
NAM-26	259 ± 56	252 ± 59	2.2 ± 0.5	2.1 ± 0.6	oc
NAM-27	83 ± 17	81 ± 17	7.2 ± 1.6	7.3 ± 1.7	in
NAM-28	94 ± 19	96 ± 21	6.3 ± 1.4	6.1 ± 1.5	in
NAM-29	115 ± 24	110 ± 24	5.2 ± 1.2	5.2 ± 1.3	in
NAM-30	86 ± 18	83 ± 18	6.9 ± 1.5	7.1 ± 1.7	in
NAM-31	153 ± 32	167 ± 38	3.9 ± 0.9	3.4 ± 0.9	in
NAM-32	80 ± 17	80 ± 17	7.5 ± 1.7	7.4 ± 1.8	in
NAM-35	176 ± 37	166 ± 37	3.3 ± 0.8	3.4 ± 0.9	in
NAM-37	177 ± 37	168 ± 38	3.3 ± 0.8	3.3 ± 0.9	in
NAM-38	139 ± 29	138 ± 30	4.2 ± 1.0	4.1 ± 1.0	in
NAM-39	141 ± 30	139 ± 31	4.2 ± 1.0	4.1 ± 1.0	in
NAM-41	173 ± 36	168 ± 38	3.4 ± 0.8	3.3 ± 0.9	in
NAM-42	91 ± 19	95 ± 20	6.6 ± 1.5	6.1 ± 1.5	in
NAM-44	499 ± 115	481 ± 128	1.1 ± 0.3	1.0 ± 0.4	in
NAM-45	444 ± 101	443 ± 116	1.2 ± 0.3	1.1 ± 0.4	in
NAM-47	109 ± 23	132 ± 29	5.5 ± 1.2	4.3 ± 1.1	in
NAM-48	167 ± 35	159 ± 36	3.5 ± 0.8	3.5 ± 0.9	in
NAM-49	375 ± 83	390 ± 99	1.5 ± 0.4	1.3 ± 0.4	in
NAM-50	83 ± 17	75 ± 16	7.2 ± 1.6	7.9 ± 1.8	in
NAM-55	508 ± 116	469 ± 124	1.1 ± 0.3	1.0 ± 0.4	oc
NAM-56	467 ± 105	443 ± 115	1.2 ± 0.3	1.1 ± 0.4	oc
NAM-59	384 ± 85	371 ± 92	1.5 ± 0.4	1.4 ± 0.4	in
NAM-60	251 ± 54	244 ± 56	2.3 ± 0.6	2.2 ± 0.6	in
NAM-61	267 ± 57	261 ± 61	2.2 ± 0.5	2.1 ± 0.6	in
NAM-62	143 ± 30	137 ± 30	4.1 ± 0.9	4.2 ± 1.0	in
NAMBG-1A	154 ± 32	138 ± 30	3.8 ± 0.9	4.1 ± 1.0	oc
NAMBG-1B	198 ± 42	178 ± 40	2.9 ± 0.7	3.1 ± 0.8	oc

[1] Limiting minimum model ages calculated using formulation of Lal (1988) assuming instantaneous exposure, no erosion, and production rates of Nishiizumi and others (1989) including 20% uncertainty in production rates; [2] limiting maximum erosion rates calculated using formulation of Lal (1991) assuming continuous exposure, steady erosion, and production rates of Nishiizumi and others (1989) including 20% uncertainty in production rates; [3] in = inselberg, oc = outcrop.

TABLE 4

Interpretation of cosmogenic nuclide data from Namibian sediment samples

Sample	Catchment Elevation (km)[1]		Area (km^2)	^{10}Be Production Rate (at g^{-1} yr^{-1})[2]			Maximum Limiting ^{10}Be model ε[6]			Maximum Limiting ^{26}Al model ε[6]		
	max	min		max[3]	min[4]	weighted[5] average	max	min	weighted[5] average	max	min	weighted[5] average
NAM-08	1.91	1.75	5.3×10^{1}	17.9	16.1	16.9	5.7	5.1	5.3	6.0	5.4	5.7
NAM-09	1.86	1.39	1.3×10^{1}	17.3	12.5	15.2	18.4	13.2	16.1	20.9	14.9	18.2
NAM-16	2.08	0.75	1.6×10^{4}	20.1	7.8	12.7	14.4	5.4	9.0	16.3	6.0	10.1
NAM-43	1.19	1.07	0.5×10^{0}	10.8	9.9	10.1	8.9	8.1	8.3	9.1	8.3	8.5
NAM-46	2.48	0.91	4.1×10^{3}	26.0	8.8	11.9	16.4	5.4	7.3	17.6	5.5	7.7
NAM-52	2.22	0.07	1.2×10^{5}	21.4	4.5	12.4	4.4	0.9	2.6	5.1	1.1	2.9
NAM-57	1.87	0.03	2.8×10^{4}	17.5	4.5	9.42	12.9	3.1	6.8	13.1	2.9	6.8

[1] Elevation taken from topographic maps; max = highest point in catchment; min = elevation of sediment sampling site; [2] assuming production rates of Nishiizumi et al. (1989) and scaling for neutrons only; [3] calculated from maximum catchment elevation; assumes all sediment is generated in the highest headwaters; [4] calculated from minimum catchment elevation; assumes all sediment is generated near sampling site; [5] weighted average is basin integrated production rate calculated by convolving basin hypsometry and production rate function at 100 to 500 meter bins (Bierman and Steig, 1996); assumes sediment is generated throughout the basin; [6] limiting model erosion rates calculated using formulation of Bierman and Steig (1996).

TABLE 5

Interpretation of cosmogenic nuclide data from Namibian clast samples

Sample	minimum limiting ^{10}Be model age (kyr)[1]	minimum limiting ^{26}Al model age (kyr)[1]	maximum limiting ^{10}Be model ε (m myr^{-1})[2]	maximum limiting ^{26}Al model ε (m myr^{-1})[2]	maximum limiting ratio model ε[3] (m Myr^{-1})	ratio model age[3,4]	minimum exposure[3,5] (kyr)	minimum burial[3,6] (kyr)	minimum total history[3,7] (kyr)
NAM-13A	266 ± 57	230 ± 53	2.16 ± 0.52	2.36 ± 0.65	1.36	750	290	200	490
NAM-13B	278 ± 60	246 ± 57	2.06 ± 0.50	2.19 ± 0.61	1.60	650	300	150	460
NAM-13C	302 ± 65	273 ± 64	1.89 ± 0.46	1.95 ± 0.56	1.80	590	320	120	440
NAM-17B	1604 ± 479	914 ± 305	0.26 ± 0.12	0.41 ± 0.23	0.10	4100	2120	370	2480
NAM-17C	1246 ± 339	810 ± 255	0.36 ± 0.14	0.49 ± 0.24	0.20	2880	1560	340	1900
NAM-17D	1795 ± 563	965 ± 331	0.22 ± 0.11	0.38 ± 0.22	0.06	4840	2420	370	2790
NAM-51A	202 ± 43	207 ± 47	2.89 ± 0.68	2.66 ± 0.71	N.A.	N.A.	N.A.	N.A.	N.A.
NAM-51C	1424 ± 407	927 ± 312	0.30 ± 0.13	0.40 ± 0.22	0.18	2990	1760	300	2060
NAM-51F	1023 ± 266	457 ± 120	0.47 ± 0.16	1.06 ± 0.37	N.A.	N.A.	1710	790	2500
NAM-58A	782 ± 192	534 ± 161	0.65 ± 0.20	0.87 ± 0.36	0.30	2270	990	400	1390
NAM-58C	318 ± 70	233 ± 56	1.78 ± 0.44	2.33 ± 0.66	0.53	1540	400	440	840
NAM-58D	633 ± 149	563 ± 155	0.83 ± 0.24	0.81 ± 0.31	1.01	960	680	110	790

N.A. = not applicable, ratio either too high or too low to make meaningful calculation; [1] single nuclide limiting model ages calculated using formulation of Lal (1988) assuming instantaneous exposure, no erosion, and production rates of Nishiizumi and others (1989); [2] single nuclide limiting model erosion rates calculated using formulation of Lal (1991) assuming continuous exposure, steady erosion, and production rates of Nishiizumi and others (1989); [3] calculated for multiple nuclide data according to methods presented in Bierman and others (1999) and using production rates of Nishiizumi and others (1989); [4] model age based on decrease in ^{26}Al/^{10}Be ratio, assumes no erosion and thus no change in production rates over time; [5] the minimum pre-burial exposure period assuming one period of surface exposure followed by burial; [6] the minimum post-exposure burial period assuming one period of surface exposure followed by burial; [7] minimum total sample history (exposure and burial) consistent with measured ^{10}Be and ^{26}Al abundances.

Fig. 2. The Namibian escarpment cut across tilted schist at the Gamsburg Pass. Road for scale in center of photo. NAM-9, collected from a stream draining this topography several kilometers south, has ^{10}Be activity equivalent to a model denudation rate of 16 m myr^{-1}, the highest denudation rate measured in this study.

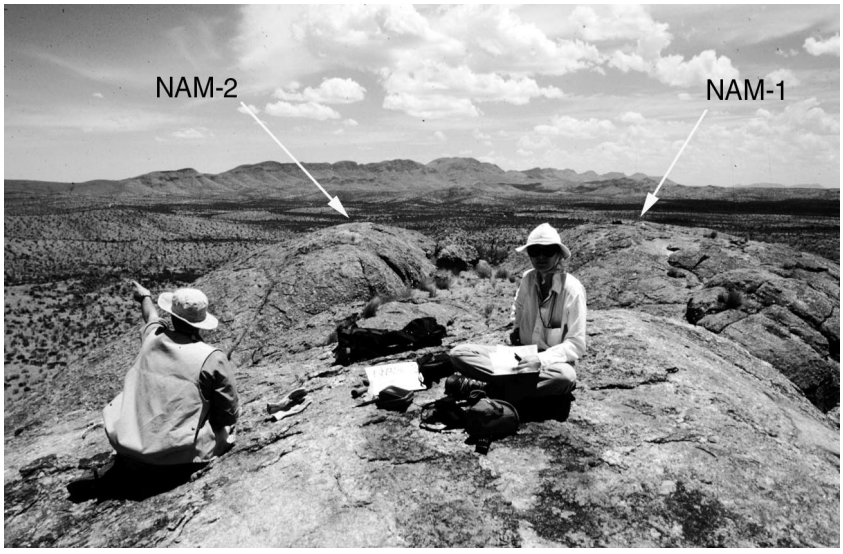

Fig. 3. View from top of inselberg, where samples NAM-1, 2, and 3 were collected, showing topography, vegetation, and rock weathering in a highland area underlain by granite and receiving 350 mm yr^{-1} of precipitation. Sign board marks the site of NAM-3. NAM-1, NAM-2, and NAM-3 have model erosion rates of 2.1, 2.5, and 3.3 m my^{-1}, respectively. Mass loss from the sampled surfaces appears to be dominated by thin sheeting.

in Namibia flow along the borders and originate elsewhere (Jacobsen, Jacobsen, and Seely, 1995). The timing of the onset of initial aridity is uncertain (Ward and Corbett, 1990). Some argue for an Eocene onset (Ward and Corbett, 1990); others suggest

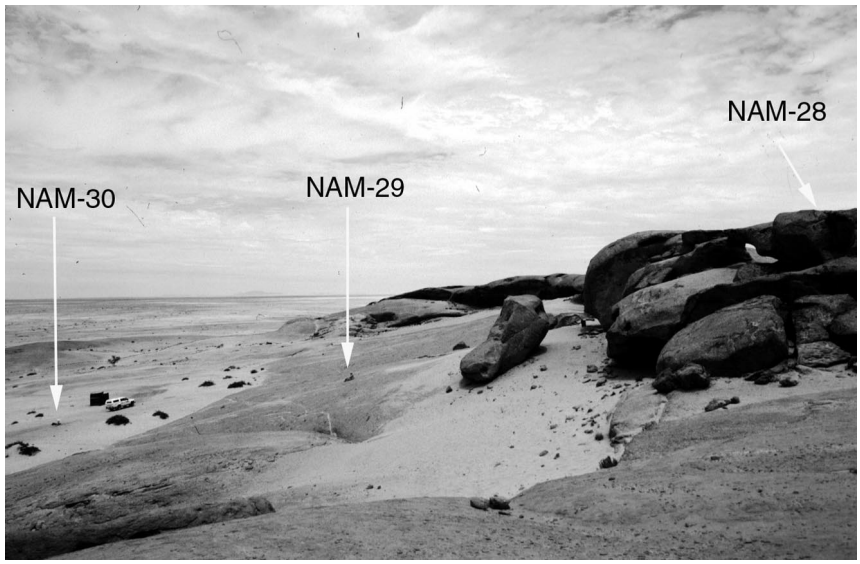

Fig. 4. Small inselberg adjacent to Vogelfederberg in the Namib desert. NAM-28, NAM-29, and NAM-30 collected from this site at locations shown on photograph. NAM-27 is from top, center of the inselberg, behind NAM-28. Vehicle for scale. All four samples had similar model erosion rates (7.2 – 5.2 m my^{-1}) and similar $^{26}Al/^{10}Be$ ratios (6.1 – 5.7); there was no isotopic indication of burial during or after exposure for any of the samples.

aridity began in the Miocene (Partridge and Maud, 1987). A variety of studies indicates some climate variability within continuing Quaternary aridity (Selby, Hendy, and Seely, 1979; Heine, 1985).

The geology of west-central Namibia is varied and influenced strongly by ancient orogenies; many of the older rocks were metamorphosed during the Precambrian, and many of the granitic rocks were intruded during the Cambrian. In the west central part of the country where we sampled, bedrock is commonly coarse crystalline gneiss and schist (Miller, 1983; Miller and Schalk, 1980). Many of these rocks are pervasively deformed. The isotopic data we present here were measured in quartz mineral separates; thus, our conclusions are most robust for the quartz-bearing lithologies in the field area.

UNDERSTANDING LANDSCAPES USING COSMOGENIC NUCLIDES

Cosmogenic nuclides, such as ^{10}Be and ^{26}Al, are produced in rock as cosmic rays, primarily neutrons, interact with atoms such as Si and O in quartz (Lal, 1988; Lal and Peters, 1967). The cosmic rays and more importantly the secondary neutron cascade are attenuated exponentially in the Earth's atmosphere and in the upper several meters of Earth's crust. Accordingly, cosmogenic ^{10}Be and ^{26}Al, produced in rocks residing near the surface, are indicators of residence time in this region of cosmogenic nuclide production (Lal, 1991). Very low nuclide production rates in terrestrial materials (10^1-10^3 atoms g^{-1} yr^{-1}) result in low nuclide concentrations and demand sensitive analytical procedures, in particular, Accelerator Mass Spectrometry (AMS), to quantify reliably nuclide abundance (Elmore and Phillips, 1987; Finkel and Suter, 1993). Chemical treatments remove nuclides produced in the atmosphere and adhered to the surfaces of mineral grains (Kohl and Nishiizumi, 1992).

Nuclide abundances are interpreted using a variety of models dependent on a variety of assumptions (Bierman, 1994). Rocks collected from rapidly exposed, non-

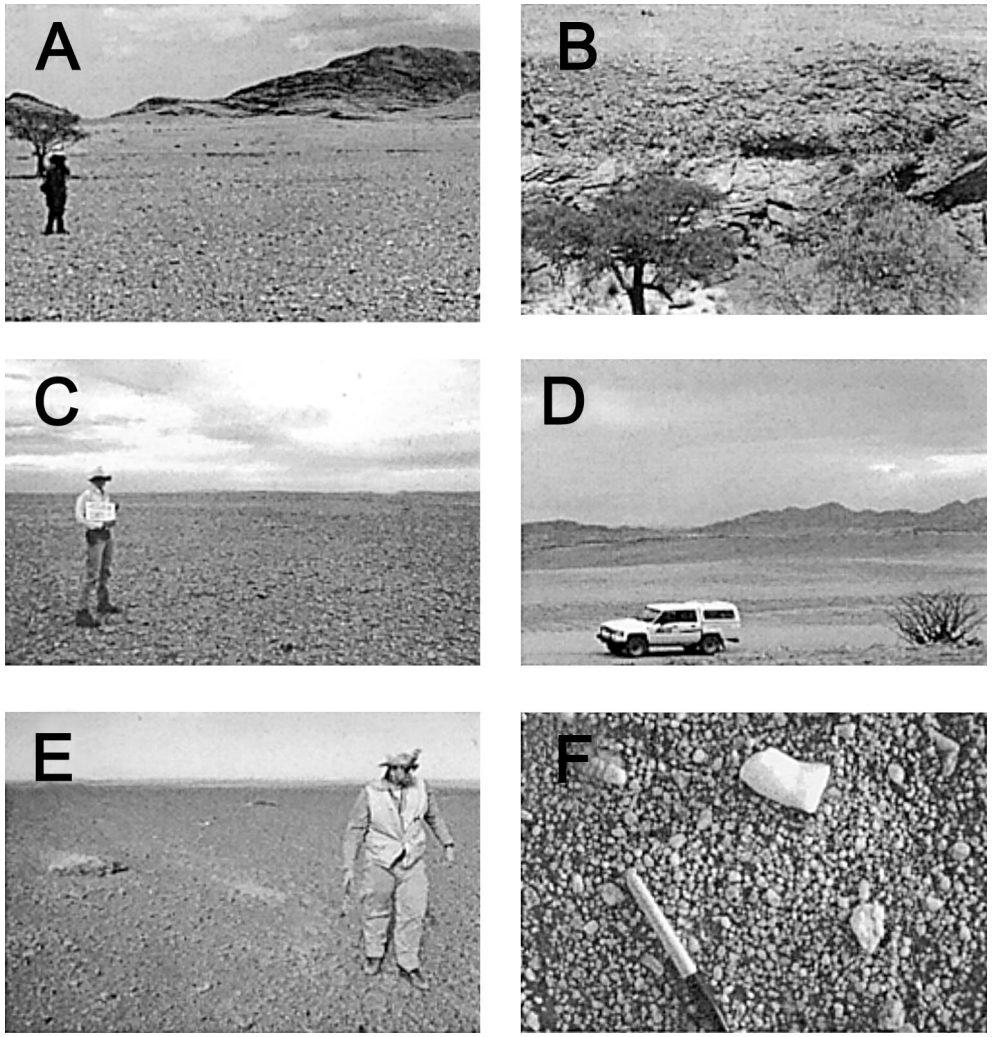

Fig. 5. Sampled gravel surfaces in Namibia. (A) Surface in the escarpment zone from which NAM-13 clasts were collected . Gneissic inselberg in background similar to that from which NAM-10, NAM-11, and NAM-12 were collected. White clasts on surface are carbonate derived from eroding petrocalcic horizon. (B) Cross-section view of NAM-13 sample site in the escarpment zone. Surface is underlain by several meters of carbonate cemented gravel, which overlies beveled bedrock; tree for scale. (C) Surface from which NAM-17 samples were collected, looking west. Samples from this surface have the greatest ^{10}Be abundance of any collected in this study, equivalent to more than 1.8 my of continuous surface exposure. Ratio data (^{26}Al/^{10}Be) suggest 3 to 5 myr histories for some NAM-17 clasts. (D) View northeast toward the escarpment and highlands from sample site NAM-17. Flat surface in middle distance is similar in elevation and morphology to the NAM-17 sampled surface. (E) Flat gravel surface (NAM-58) near the coast. Sand collected by vegetation shows one way in which burial, detected isotopically, may occur for clasts on Namibian gravel surfaces. (F) Ventifacted clast, similar to those analyzed, in place on desert surface at site NAM-51; pen for scale.

eroding surfaces may be dated (Gosse and others, 1995; Stone and others, 1996; Stone, Ballantyne, and Fifield, 1998); whereas, nuclide abundance in samples collected from steadily eroding surfaces may be used to calculate maximum limiting erosion rates (Bierman and others, 1995; Bierman and Turner, 1995; Bierman, 1994; Lal, 1991; Nishiizumi and others, 1986, 1991). Nuclide abundance in sediments collected from

streams and rivers is proportional to the average erosion rate integrated over the drainage basin (Bierman and Steig, 1996; Brown and others, 1995b; Granger, Kirchner, and Finkel, 1996). If sediment residence times are short, such nuclide abundances equate to rates of bedrock lowering. Nuclides measured in colluvium and in samples collected from sedimentary deposits can be used to understand lowering, deposition, and sediment transport rates across the landscape (Clapp and others, 2000, 2001; Clapp, Bierman, and Caffee, in press; Nichols and others, in press; Small, Anderson, and Hancock, 1999; Heimsath and others, 1999, 2000).

Analysis of paired nuclides having different half-lives, such as ^{10}Be ($t_{1/2}$ = 1.5 Ma) and ^{26}Al ($t_{1/2}$ = 0.7 Ma) can provide additional information about sample history (Bierman and others, 1999; Klein and others, 1986; Nishiizumi and others, 1991). Measured ^{10}Be/^{26}Al ratios reflect the ^{10}Be/^{26}Al production ratio, the contrast in nuclide half-lives, and each sample's particular geologic history in terms of burial and exposure. Samples that are continuously exposed will have a predictable nuclide abundance and ^{10}Be/^{26}Al ratio (Klein and others, 1986; Nishiizumi and others, 1991). However, if a bedrock outcrop, boulder, clast, or sediment has been buried and shielded from cosmic rays during or after exposure, the ^{10}Be/^{26}Al ratio will deviate from the predicted value and drop as the nuclide with the shorter half-life (^{26}Al) decays more quickly. Such an approach can be used to set lower limits on the sample's total history of exposure and burial and has been employed for dating cave sediments (Granger, Kirchner, and Finkel, 1997) and glaciated surfaces (Bierman and others, 1999). However, ^{10}Be and ^{26}Al can be used to identify complex exposure histories only in samples that have been buried for $>10^5$ yrs, a significant part of the ^{26}Al half-life (0.7 Ma).

METHODS

To characterize the rate at which rock weathers and the landscape of west central Namibia changes, we collected and analyzed three types of samples: sediment from active stream channels, clasts preserved on very low-relief geomorphic surfaces, and rock (primarily granite and gneiss). Samples were collected in December, 1998. Locations were determined using a hand-held, Garmin GPS (table 1).

We collected coarsely crystalline, quartz-bearing rock samples from bare bedrock outcrops along three transects from the highlands to the coast (fig. 1; tables 1 and 3). We sampled mostly rocks mapped as granite (Miller and Schalk, 1980); however, some of the samples exhibit strong fabrics and are more gneissic in character. In a few places where granite did not crop out, we collected quartzite from the meta sedimentary cover and quartz veins from the gneiss (fig. 6). We sampled primarily the tops and flanks of granitic inselbergs or isolated rocky hills, to characterize the rate at which bare rock erodes (figs. 3 and 4).

We collected sediment samples both from rivers draining large basins (10^3-10^4 km^2) and from streams draining small catchments (10^0-10^1 km^2). We sampled sediment from the dry channels of four through-flowing rivers which originate on the highlands and cross the escarpment, the Ugab, the Kahn, the Omaruru, and the Kuiseb (fig. 1 and table 4). We also sampled three small catchments. One small catchment was located above the escarpment and drains granitic outcrops on the Weissenfels farm; one stream drains schist of the escarpment near Gamsburg Pass; one stream drains granitic terrain at Ranch Amieb on the coastal plain (fig. 7). All channels we sampled were dry as is typical in Namibia where streams and rivers flow quite rarely. Samples were integrated by collecting across the channel and we analyzed only the 250 to 800 mm sand fraction, because experiments in other arid regions show no dependence of nuclide concentration on grain size (Clapp and others, 2000, 2001; Clapp, Bierman, and Caffee, accepted).

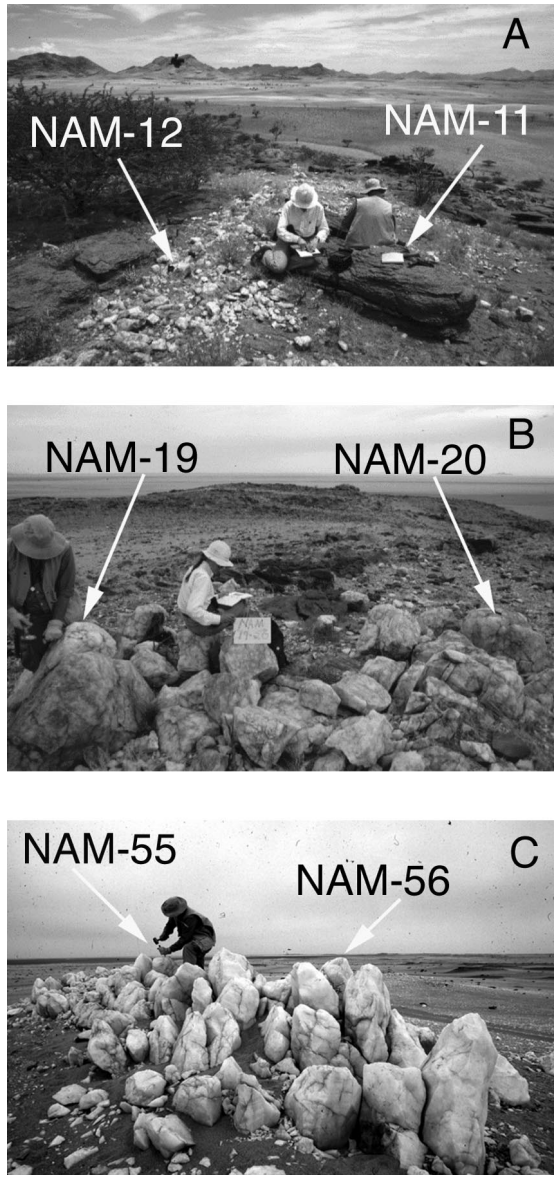

Fig. 6. Quartz veins sampled in Namibia. (A) Exposure of quartz vein sample NAM-12 at top of gneissic hill. NAM-11 is gneiss sample on adjacent boulder; these samples had model erosion rates of 5.4 and 4.1 m my^{-1}, respectively. Erosion of this and other thin, fractured quartz veins is controlled by mass loss rate of surrounding gneiss. (B) Exposure at top of large hill on the coastal plane in pegmatite (NAM-19 and -20); samples have erosion rates of 2.5 and 2.3 m my^{-1}, respectively. (C) Exposure at top of small hill near the coast; samples NAM-55 and –56 have very low erosion rates of 1.1 and 1.2 m my^{-1}, respectively.

We collected clasts from four different geomorphic surfaces, one within and three below the escarpment zone (table 5). All surfaces were covered by gravel and sand, were extremely flat, and had little or no vegetation (fig. 5). On each surface, we collected three clasts of quartz or chert; each clast was selected because it was large enough to analyze individually, 5 to 10 cm in each dimension. All clasts were

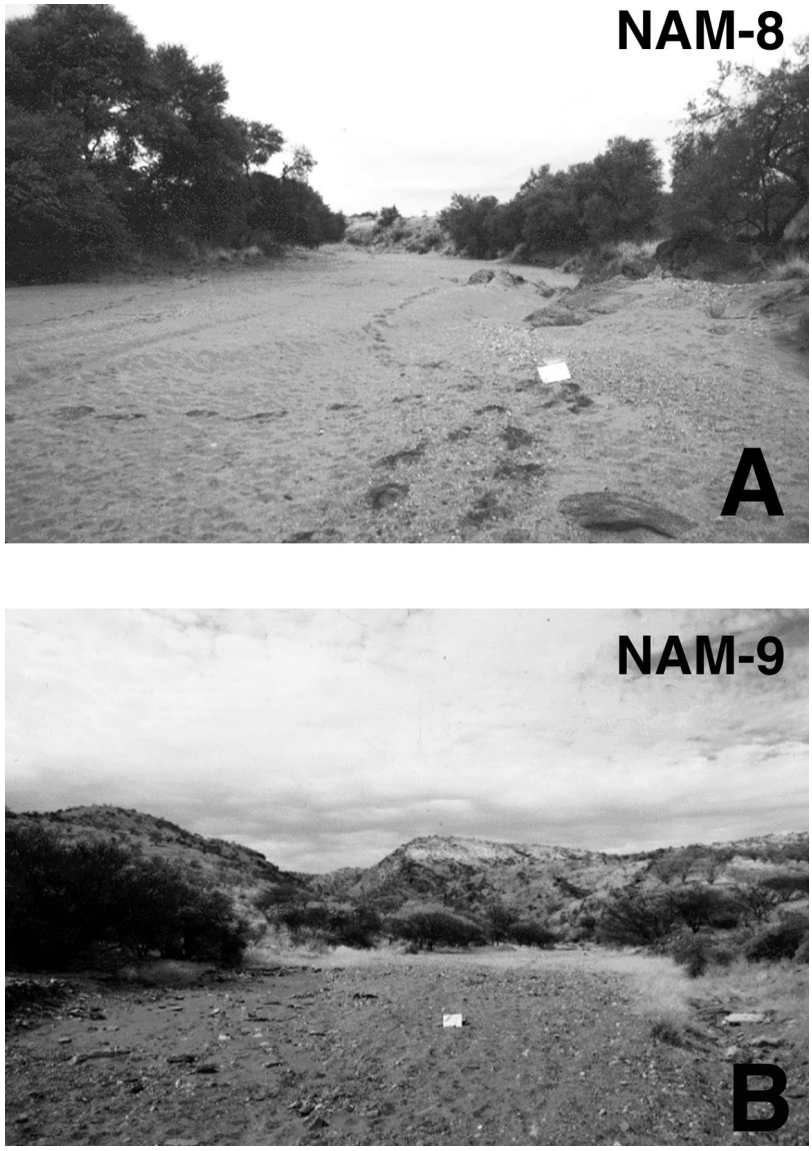

Fig. 7. Sample sites in small catchments. (A) NAM-8, Weissenfels Farm, on highlands above the escarpment where the channel drains a landscape of granitic inselbergs. ^{10}Be activity in channel sediments suggests a basin scale erosion rate of 5 m my^{-1}. (B) NAM-9, an unnamed stream with headwaters on the escarpment, carries sediment for which the ^{10}Be activity suggests a basin-scale erosion rate of 16 m my^{-1}.

ventifacted and wind polished; however, we cannot determine the amount of mass lost from the geomorphic surfaces by all processes and from the clasts by wind erosion (fig. 5F).

Samples were returned to the University of Vermont and treated to isolate 20 to 40 grams of pure quartz. Clasts and rock samples were crushed and the sediment samples were sieved. Samples were given a single ultrasonic etching in 6 N HCl followed by repeated etchings in 1 percent HF and HNO_3 (Kohl and Nishiizumi, 1992). For

samples with significant mafic minerals remaining after etching, we used tungstate-based heavy liquids to further isolate quartz by density separation. Chert samples (NAM-58A,C) were etched for shorter periods of time.

After one additional HF/HNO_3 etching, samples were dissolved in HF along with 250 μg of Be-carrier (SPEX brand) and, if needed, Al carrier to bring the total quantity of ^{27}Al to >2000 μg. Aliquots were taken directly from the HF solution for measurement of stable Al. Total Al was quantified by ICP-AE (Inductively couple Argon Plasma Spectrometry, Optical Emission) using duplicate measurements of multiple aliquots normalized to four internal standards run as unknowns. Precision of total Al measurements is better than 2 percent. Solutions were purified by anion exchange as well as pH-specific precipitation. Be and Al were separated by cation exchange, precipitated as hydroxides, and burned to produce oxides.

The oxides were mixed with Ag and packed into targets in a HEPA-filtered glove box at the University of Vermont. Targets were analyzed by AMS (Accelerator Mass Spectrometry) at Lawrence Livermore National Laboratory (LLNL). Analyses were normalized to standards either prepared by K. Nishiizumi or prepared by LLNL and referenced to standards prepared by K. Nishiizumi. Blank corrections (typically < 1 percent) were made based on the analysis of full process blanks run with each batch of seven samples. Analysis of one laboratory replicate, NAM-7X, suggests that our data are reproducible to several percent (table 2).

DATA ANALYSIS

We reduce data as maximum limiting erosion rates and minimum limiting surface exposure ages using accepted interpretive models for cosmogenic nuclides (tables 1-5; Bierman and Steig, 1996; Lal, 1988, 1991). Field observations suggest that the erosion model is more valid than the exposure case; however, we quote the results of both calculations for comparison. Some clast samples, for which cosmogenic nuclide ratio data indicate complex exposure histories, are considered using the methodology presented in Bierman and others (1999). We normalize measured nuclide abundances to sealevel and high latitude using data of Lal (1991), considering only neutrons. Such calculations assume that muon-induced production is inconsequential in our samples, an assumption supported by recently published data (Brown and others, 1995a; Granger and Smith, 2000).

To facilitate comparison with earlier studies, we make our calculations using a sealevel, high latitude ^{10}Be production rate of 6.0 atoms g^{-1} yr^{-1} (Nishiizumi and others, 1989) acknowledging that this rate is uncertain and may be 10 to 20 percent too high (Clark, Bierman, and Larsen, 1995). We propagate a 20 percent uncertainty in production rates when making erosion rate and exposure age calculations. This uncertainty is appropriate when comparing our nuclide-based rates and dates with those generated by other geochronologic systems. Because production rate inaccuracies are in large part systemic, the uncertainty in nuclide abundance (typically only several percent) is more representative of uncertainty when comparing cosmogenically-based rates between sites in Namibia.

In addition to production rate uncertainties, model erosion rates and exposure ages calculated from cosmogenic nuclide abundances are beholden to a variety of assumptions including uniform and steady erosion (Lal, 1991), the accuracy of production scaling factors for altitude and latitude (Lal, 1988; Dunai, 2000; Desilets and Zreda, 2000), and the intermittent covering of outcrops by windblown sediment and soil. Although average, fully propagated, analytic precision for our samples is high (3 and 5 percent for ^{10}Be and ^{26}Al, respectively), the uncertainty of calculated ages and erosion rates is likely several times higher. Interpreting $^{10}Be/^{26}Al$ ratio data (table 5) is more uncertain; see detailed discussion of error propagation in Gillespie and Bierman (1995) and Bierman and others (1999). Interpreting nuclide abundances in sediments

as basin-scale erosion rates is also beholden to many assumptions including uniform quartz distribution, sediment storage times less than nuclide half-lives, and a steady state landscape (Granger, Kirchner, and Finkel, 1996; Brown and others, 1995b; Bierman and Steig, 1996). For large and steep basins, the dominant uncertainty is the location (altitude) from which the analyzed quartz is derived. We consider this uncertainty by calculating erosion rates using several limiting cases (table 4).

DATA AND INTERPRETATIONS

Rock Surfaces

The 47 bare rock outcrops that we sampled in Namibia are eroding slowly, on average 3.5 ± 1.8 m my^{-1} (table 3 and fig. 8). Using the assumption of uniform erosion (loss of mass by granular disintegration and thin spalling (Lal, 1991) as we observed at most Namibian outcrops) measured nuclide abundances imply maximum limiting erosion rates ranging from 1.1 to 7.5 m my^{-1} (NAM-55 or 44 and NAM-32, respectively), the equivalent of 80 to 500 kyr of continuous surface exposure. NAM-55 and NAM-44, the most highly dosed and presumably most stable rock surfaces, are a quartz vein near the coast (fig. 6) and an inland granite, respectively. NAM-32, the bare rock sample in which we measured the lowest nuclide abundance and thus calculated the highest erosion rate, was collected from a granitic outcrop, also near the coast but 225 km farther south (table 1 and fig. 1).

Lack of lithologic control on nuclide abundance and model erosion rates.—Lithology appears to exert little control on the erosion rate of subaerially exposed quartz-bearing rocks in Namibia. The average erosion rates for exposed granite (3.7 ± 2.1 m my^{-1}, n = 31), gneiss (3.7 ± 0.7 m my^{-1}, n = 9), and quartzite outcrops (3.6 ± 1.2 m my^{-1}, n = 2) sampled are indistinguishable. The average erosion rate for large outcropping quartz veins (2.5 ± 1.7 m my^{-1}, n = 5; fig. 6) is lower than those calculated for all other lithologies, more substantially so (1.8 ± 0.7 m my^{1}, n = 4) if we do not include NAM-12 in the statistical analysis because it was a narrow (<1 m wide) vein (fig. 6A) entirely surrounded by gneiss weathering at 4.1 m my^{-1}.

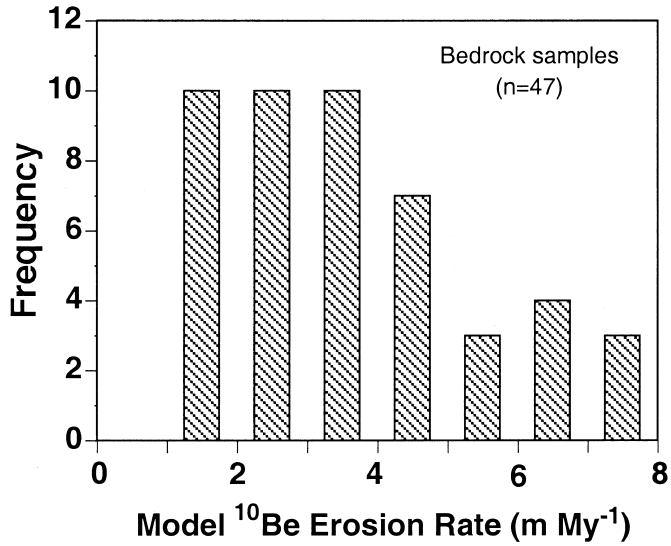

Fig. 8. Summary histogram of bare rock model erosion rates for Namibia, n=47, calculated from ^{10}Be activity using steady erosion model of Lal (1991). Overall mean rock erosion rate is 3.5 ± 1.8 m my^{-1}.

Lack of relationship between bare rock erosion rates, climate, and landscape position.— Analyses of 47 samples collected from bare rock surfaces demonstrate that rock erosion rates in Namibia are quite low, variable, and do not change systematically across wide gradients of three, well correlated landscape-scale parameters: elevation, mean annual precipitation, and distance from the coast (fig. 9). There is no significant

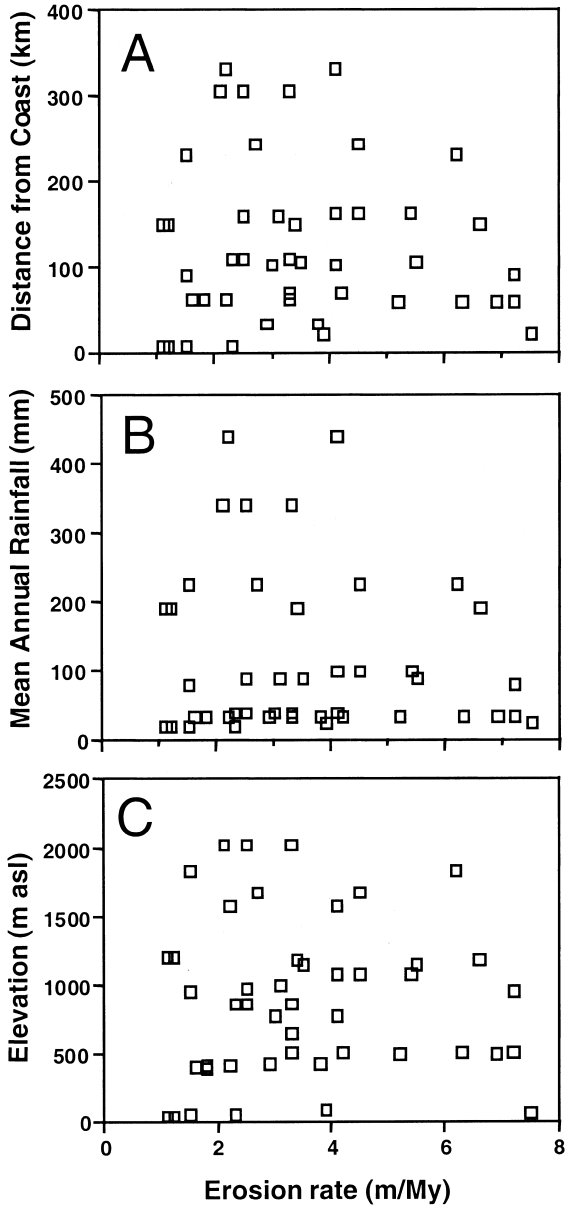

Fig. 9. There is no relationship between bare rock erosion rates and gradients in three landscape-scale parameters. Regression analyses of all three graphs indicated correlation coefficients, r^2, < 0.01. (A) Sample site distance from coast, a proxy for fog frequency and salt abundance. (B) Estimated annual rainfall at sample sites (Jacobsen, Jacobsen, and Seely, 1995). (C) Sample site elevation above sea level.

difference between the average rate of denudation calculated for exposed bedrock samples collected above (3.2 ± 1.5, n = 9) and below (3.6 ± 1.9, n = 38) the Namibian Escarpment.

Lack of intermittent burial and complex exposure history.—Taken together, ^{26}Al and ^{10}Be data indicate that bare rock surfaces across Namibia have nuclide concentrations most consistent with simple exposure histories, either continuous surface exposure or steady erosion. All bedrock samples have nuclide ratios between 5.0 and 6.4; when plotted on a two isotope diagram, none has a nuclide abundance (at 2 sigma) indicative of extended burial during or after cosmic ray exposure (fig. 10). Only 2 of 47 samples plot more than one sigma below the line of steady erosion; another two samples plot more than one sigma above the constant exposure line. The statistical consistency of all 47 paired nuclide measurements with the assumption of steady erosion or constant exposure, as represented by the intersection of sample points at two sigma uncertainty with the scythe-shaped window in figure 10, suggests that mass loss from eroding surfaces is occurring in pieces considerably thinner than the scale depth of cosmic ray penetration, 165 g cm^{-2} or about 60 cm of rock (compare Bierman and others, 1999; Cockburn, Seidl, and Summerfield, 1999; Lal, 1991).

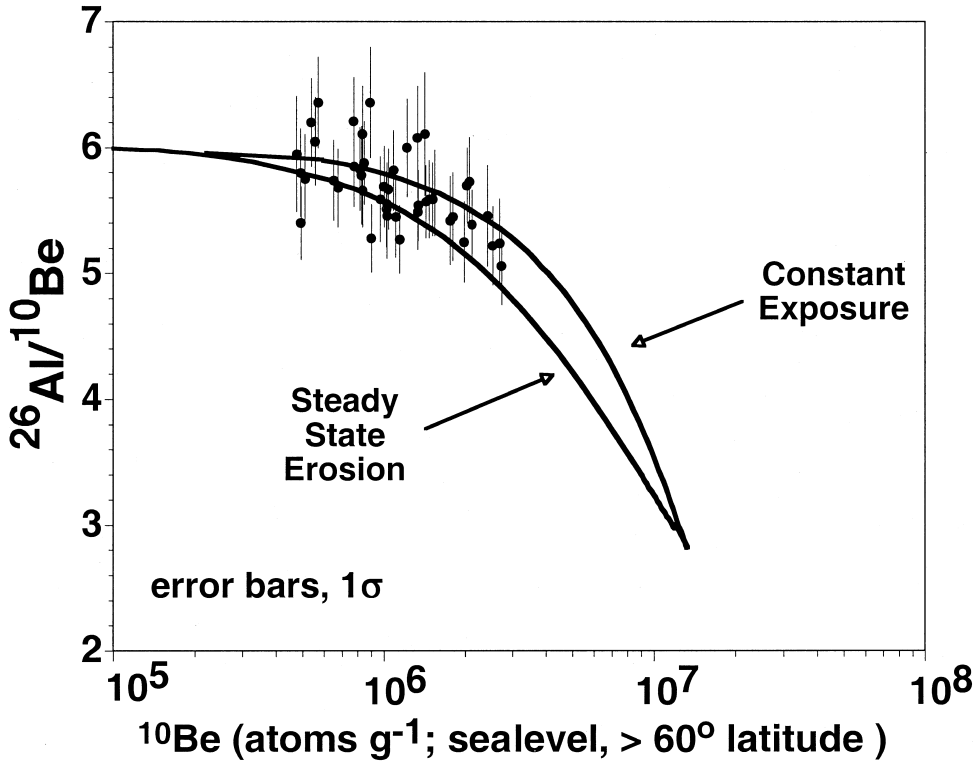

Fig. 10. Two isotope diagram for 47 exposed bedrock samples collected in Namibia. Scythe-shaped window indicates region where samples that have either been continuously exposed or steadily eroding should plot. Samples with history of burial during or after exposure will plot below line of steady state erosion endpoints that defines the bottom of the scythe-shaped window. All but four Namibian bedrock samples plot within 1 sigma of the region defined by models of constant exposure and steady erosion without complex exposure histories indicating that there is no robust evidence for burial of any sampled surface. Two of the samples plotting below the simple exposure history window were collected from the top of a quarry wall (NAMBG-1 and NAMBG-2) where a thin veneer of regolith may have been removed by quarry operations prior to our sampling; the third, NAM 50, was collected from the top of an inselberg where there is no evidence for prior burial or episodic loss of mass in thick sheets.

The isotopic indication of continuous exposure for our sample set is particularly striking at a site where some intermittent burial might be expected. Vogelfederberg is a massive granitic inselberg rising about 100 m from the beveled bedrock plains of the central Namib Desert. Because the main inselberg had been sampled by Cockburn, Seidl, and Summerfield (1999), we sampled a smaller, unnamed but adjacent inselberg (fig. 4). To determine the inselberg's exposure and erosion history, we collected two samples from the top (NAM-27 and NAM-28), one sample from a side slope (NAM-29), and one sample from the bare rock pediment at the base of the landform (NAM-30).

All four inselberg samples have similar nuclide abundances (0.49 − 0.68 ^{10}Be atoms g^{-1}) and none, including the platform sample which rises just centimeters above the grus-covered plain, shows evidence for burial (^{26}Al/^{10}Be, 5.7-6.1). There is no elevational pattern in either the nuclide ratios or abundances; the pediment sample has nuclide abundances similar to the other three suggesting that it has not been covered significantly in the past by sand, grus, or colluvium which would lower both nuclide abundances and the ratio, ^{26}Al/^{10}Be. On average, the inselberg we sampled is eroding about 6.5 m my^{-1} (n = 4, ^{10}Be only) similar to the rate of 5.5 m my^{-1} (n = 2, ^{10}Be only) estimated for adjacent Vogelfederberg (Cockburn, Seidl, and Summerfield, 1999).

Spatial variability of nuclide abundance and model erosion rates.—In many cases, samples collected near one another contain similar nuclide abundances. Samples NAM-10, -11, and -12 were collected from the side and top of a gneiss hill (fig. 6A). All are eroding at similar rates (4.5, 4.1, and 5.4 m my^{-1}). Two gneiss inselbergs (NAM-14 and NAM-15), separated by almost a kilometer, have similar nuclide abundances and thus model erosion rates (3.1, 2.5 m my^{-1}, respectively). NAM-19 and NAM-20, two samples collected 4.5 m apart in a ridge-top quartz vein have very similar nuclide abundances and model erosion rates, 2.3 and 2.5 m my^{-1} as do two other samples from a massive quartz vein near the coast (fig. 6; NAM-55 and -56; 1.1 and 1.2 m my^{-1}, respectively). Samples (NAM-37 and -38) collected from within 4 m of each other on the top of Rossingberg, a gneiss dome, have similar nuclide abundances and calculated erosion rates (3.3 and 4.2 m my^{-1}), as does a sample 30 m away (NAM-39, 4.2 m my^{-1}). Another pair of measurements, made at a low granite dome near Mirabib Inselberg (Cockburn, Seidl, and Summerfield, 1999) tells a similar story. Two samples (NAM-21 and -22) were collected 20 m apart from two adjacent low (8 m high) domes. The first sample has slightly higher nuclide abundance than the second resulting in model erosion rates of 3.0 and 4.1 m my^{-1}, respectively, similar to the average rate measured for the larger, adjacent Mirabib by Cockburn, Seidl, and Summerfield (1999), 3.9 m my^{-1} (n = 2, ^{10}Be only).

In other cases, nuclide abundances vary significantly between adjacent samples. For example, samples NAM-1, NAM-2, and NAM-3 were collected from within 20 m of each other at the top of a granitic inselberg (fig. 3); nuclide abundances and thus calculated erosion rates (2.1, 2.5, and 3.3 m my^{-1}) vary 50 percent. NAM-4 and NAM-5, collected from the tops of two small, adjacent quartzite hills, also have significantly different model erosion rates (2.7 versus 4.5 m my^{-1}). Two samples (NAM-47 and -48) collected within 24 m of each other on a small dome near Spitzkoppe have significantly different model erosion rates, 5.5 and 3.5 m my^{-1}, respectively. Samples NAM-6 and NAM-7, collected from different parts of a large granitic inselberg capped by spheroidal boulders and separated by tens of meters, have nuclide abundances that vary more than three fold. NAM-49 and NAM-50 were collected within 3 m on the top of an inselberg and have a 4-fold difference in ^{10}Be activity. To generate such differences by episodic exfoliation of granitic slabs would require removal of material on the scale of 25 to 100 cm, greater than the thickness of most pieces currently being shed from the outcrops we sampled.

Samples of similar lithologies only several kilometers away sometimes have significantly different nuclide abundances and erosion rates. At Ranch Amieb, we collected pairs of nearby samples at two sites separated by only several kilometers. NAM-41 and -42, collected from two nearby (10 m) bouldery surfaces above Phillips Cave, have nuclide abundances that differ by a factor of two and allow calculation of erosion rates of 3.4 and 6.6 m my^{-1}, respectively. The other two samples (NAM-44 and -45), collected from a meter-thick weathered granite slab and a smooth, bare granite surface 32 m away, have high and similar nuclide abundances suggesting slow erosion rates of 1.1 and 1.2 m my^{-1}.

Stability of the Namib Sand Sea's northern margin.—The Namib Sand Sea extends several hundred kilometers along the southern Atlantic coast and contains dunes hundreds of meters high. Currently, its northern margin is defined by the channel of the Kuiseb River; other evidence (Ward, 1987) suggests that the northern margin has been stable during at least the late Pleistocene.

Four cosmogenic nuclide samples (NAM-23 to 26), collected in a kilometer-long transect stretching north of Gobabeb and away from the sand sea margin, suggest that the northern margin of the Namib Sand Sea has not moved north of the Kuiseb River for $\geqslant$100 ky (fig. 11). All four granitic outcrops have similar nuclide abundances (1.47-1.96 $\times$ 10^6 ^{10}Be atoms g^{-1}) and similar $^{26}Al/^{10}Be$ ratios (5.25-5.59); all samples are compatible with continuous surface exposure and no significant periods of burial. If the Sand Sea had expanded northward and buried the outcrops for significant periods of time (>100 ky), we would detect such burial in lowered $^{26}Al/^{10}Be$ ratios. Furthermore, the lowest outcrop (NAM-23), which is also closest to the river and to today's dune field, would be most likely to be buried and thus would

Fig. 11. NAM-23 sample site with dunes of the Namib sand sea in the background beyond the research station at Gobabeb. In the middle ground, are outcrops surrounded by a thin cover of windblown sand. NAM-23 is the closest outcrop to the Kuiseb River and the sand sea of the four outcrops we sampled at Gobabeb. It, like the other three, show no isotopic evidence for burial by sand thus suggesting that the northern margin of the sand sea has not moved north for at least much of the Pleistocene.

have the lowest nuclide abundance and ratio. However, the nuclide abundance and $^{26}Al/^{10}Be$ ratio measured in this sample are not significantly different from those measured in the three nearby Gobabeb samples.

Sediments

We analyzed ^{10}Be and ^{26}Al in 7 samples of fluvial sediment; from most of these data, we estimate basin-scale rates of erosion higher than those estimated from bare rock surfaces. Our findings are similar to the results of Small, Anderson, and Hancock (1999) and Clapp and others (2000, 2001) who found that as a whole bedrock outcrops were more stable than drainage basins as a whole. Ratio data ($^{26}Al/^{10}Be$; fig. 12) for samples from the two largest basins (10^4-10^5 km^2) are consistent with steady erosion (NAM-52 and NAM 57); three other samples from small and intermediate size basins (10^0–10^3 km^2) plot about 1 sigma below the line of steady erosion endpoints indicating some loss of ^{26}Al by decay during storage or excavation of material from depth. Two samples, NAM-9 and NAM-16, plot 2 sigma below the line of steady erosion. Because some sediment samples show a loss of ^{26}Al in comparison to ^{10}Be, we use only the ^{10}Be data (because of this nuclide's longer half-life) to calculate maximum limiting basin-

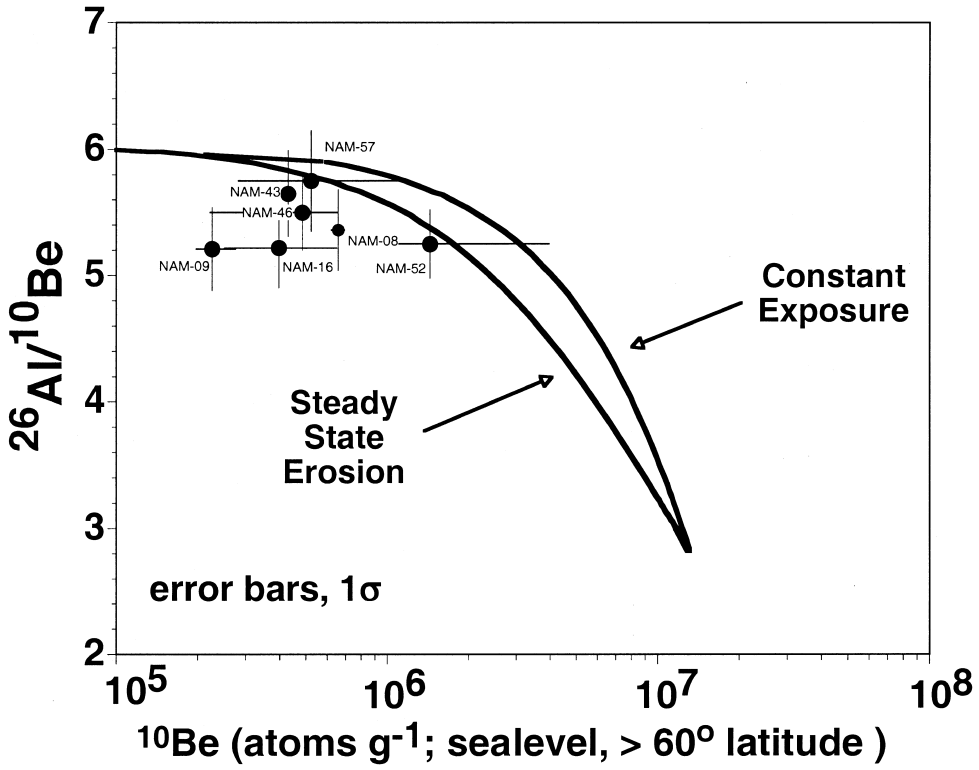

Fig. 12. Two isotope diagram for seven sediment samples collected in Namibia shows evidence for loss of ^{26}Al by decay in some samples. Such loss could result from sediment storage in the drainage basin or from erosion of material dosed under a cover of soil or sediment. Two samples, collected from the largest rivers sampled near where they reach the coast (NAM-52 and NAM-57), plot near the line of steady erosion endpoints. The other samples plot significantly to the left and below the envelope defined by simple surface exposure and steady erosion. Vertical bars represent analytical error in ratio data. Horizontal bars are the range of normalized ^{10}Be activities considering the possible source elevation of fluvially transported quartz. See table 4 for details.

scale lowering rates. We do this because sediment samples are an amalgamation of many grains, each with its own idiosyncratic history; thus, one cannot correct for the decay of a radionuclide (Brown and others, 1995b; Granger, Kirchner, and Finkel, 1996; Bierman and Steig, 1996), and the ^{26}Al data cannot be interpreted quantitatively.

Because we do not know the distribution of quartz throughout the contributing watersheds, we present three different estimates (table 4) for basin scale erosion rates calculated using minimum nuclide production rates (assuming all sediment is generated at the sample site elevation), maximum possible production rates (assuming all sediment is generated at the highest point in the catchment), and an altitude/area weighted average production rate calculated by digitizing topographic maps at 100 to 500 meter contour intervals (depending on the size and relief of the basin) and calculating production rates for the mid-point of each interval (table 4). The weighted average calculation for nuclide production rates is most reasonable given the wide distribution of quartz-bearing rocks in all sampled basins; thus, we use this production rate calculation in the discussion of model erosion rates that follows.

The data from four large rivers (NAM-16, -46, -52, and -57) suggest that on average, the Namibian landscape is lowering 6.4 ± 2.9 m my^{-1} with calculated, basin-scale erosion rates ranging between 3 and 9 m my^{-1}. Small basin sediment data suggest that basin scale erosion rates above (NAM-8; 5.3 m my^{-1}) and below (NAM-43; 8.3 m my^{-1}) the escarpment are similar and are, respectively, 55 percent to 130 percent higher than average erosion rate for bare rock surfaces above and below the escarpment. The spatially integrated erosion rate for a 13 km^2 basin (NAM-9) that heads on the escarpment and is underlain by schist is 16 m my^{-1}, much higher than any other erosion rate determined by this study and likely the result of the more rapidly eroding steep escarpment slopes (figs. 2 and 7B) or the more friable, less resistant nature of the schist. The nuclide abundance in Omaruru River sediment (NAM-52) is higher than in all other rivers and higher than many bedrock samples.

Clasts

Clasts, collected from desert surfaces and analyzed individually, have the highest nuclide abundances of all Namibian samples we measured. Maximum ^{10}Be abundance in clasts collected from coastal plain surfaces increases with elevation although there is significant variance in nuclide abundance at each coastal plain sample site (fig. 13A). Single nuclide minimum model exposure ages, calculated directly from ^{10}Be abundance and assuming no inheritance from prior exposure, approach 1.8 my for some samples (NAM-17D) implying exceptionally long near-surface residence times for individual clasts (table 5 and figs. 13B). If we assume that clast nuclide abundance is controlled by the stability of the geomorphic surface upon which the clast lies, then single nuclide model maximum erosion rates for clasts (and by analogy the geomorphic surfaces) are as low as 0.22 m my^{-1} (fig. 13C). Model minimum clast exposure ages generally increase and erosion rates generally decrease with distance from the coast and elevation (fig. 13B and C) suggesting that inland surfaces are either older or more stable. Samples collected within the escarpment zone (NAM-13) in general have the lowest and most consistent nuclide abundances and model ages (fig. 13A and B).

Considering ^{26}Al and ^{10}Be abundances together suggests that clasts on Namibian gravel surfaces have varying, complex, and extremely long total exposure histories including episodes of exposure, burial, and re-exposure. When evaluated using the two isotope plot, which graphically portrays if a sample has been buried during or after exposure, only 6 of the 12 clasts have nuclide abundances consistent at 2 sigma with a simple exposure history (fig. 14). Clast samples are clearly very much different in their ^{26}Al and ^{10}Be abundances, their ^{26}Al/^{10}Be ratios, and thus their geomorphic histories than the bare rock outcrops and fluvial sediments that we sampled (figs. 10 and 12).

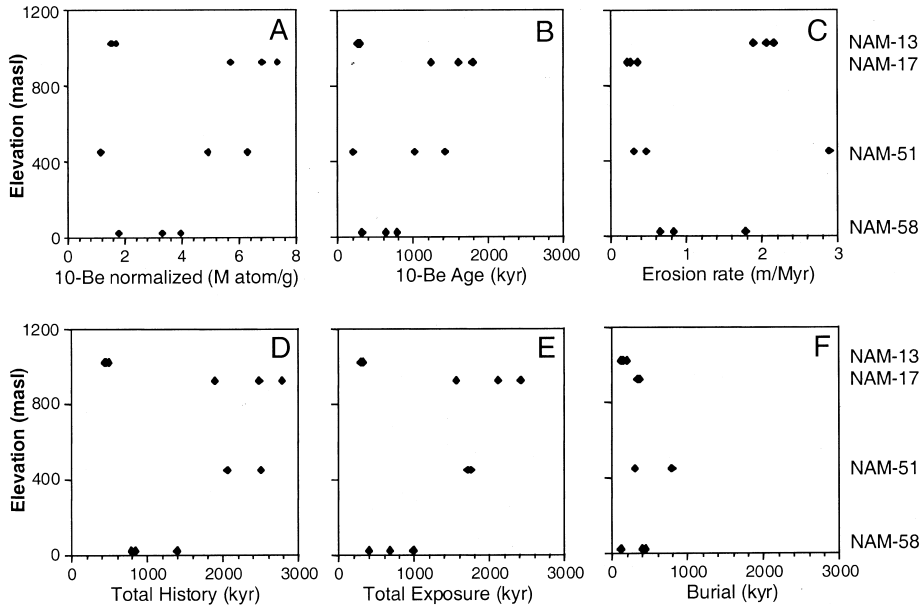

Fig. 13. Namibian clast data as a function of elevation. Nuclide abundance and surface age/stability appear to increase with elevation excepting site NAM-13, which is actively eroding as nearby gullies cut into the escarpment zone landscape. (A) Normalized ^{10}Be abundance (sea-level, high latitude). (B) ^{10}Be model exposure ages for clasts assuming no inheritance from prior exposure and no clast erosion. (C) Maximum limiting erosion rate for surface allowed by ^{10}Be clast data assuming that clasts, and the geomorphic surface upon which they sit, lower together. (D) Minimum total clast history (burial and exposure) determined from ^{26}Al/^{10}Be ratio data (Bierman and others, 1999). (E) Total minimum surface exposure history determined from ^{26}Al/^{10}Be ratio data (Bierman and others, 1999). (F) Minimum total burial history determined from ^{26}Al/^{10}Be ratio data (Bierman and others, 1999).

Modifying the methodology of Bierman and others (1999) for interpreting sample histories from measured ^{26}Al/^{10}Be ratios, we calculate total minimum sample histories for samples that plot below the simple exposure envelope (table 5 and fig. 13D). Such histories are a model construct; they are non-unique solutions that provide only the shortest possible near-surface history for each clast including a minimum time of surface exposure (fig. 13E) and a minimum time of burial and cosmic-ray shielding (fig. 13F) required for the sample to reach its measured abundance of ^{26}Al/^{10}Be.

Using an iterative solution to generate synthetic histories consistent with both measured ^{26}Al and ^{10}Be nuclide abundances (Bierman and others, 1999), we find that clasts from Namibian gravel surfaces have minimum initial surface exposure times that range from 0.3 to 2.4 my (fig. 13E); minimum complete burial times that range from 0.1 to 0.8 my (fig. 13F), and total, minimum near-surface histories that range from 0.4 to 2.8 my (fig. 13D). Total exposure and total clast histories rise inland; burial times appear random as might be expected if burial is caused by bioturbation or small shifting sand dunes such as we observed near NAM-58.

One can also interpret the clast data using the measured ratios (^{26}Al/^{10}Be) to calculate minimum total exposure times or maximum permissible erosion rates under a cover that absorbs neutrons (Bierman and others, 1999, fig. 3C). Such calculations generate extremely low erosion rates, some less than 0.1 m my^{-1} and extremely long total exposure times, nearly 5 my, implying, as all other model analyses have, exceptional stability for these clasts. Such long total histories and low erosion rates are compatible with both the preservation of the gravels and their suspected Miocene age (Ward, 1987).

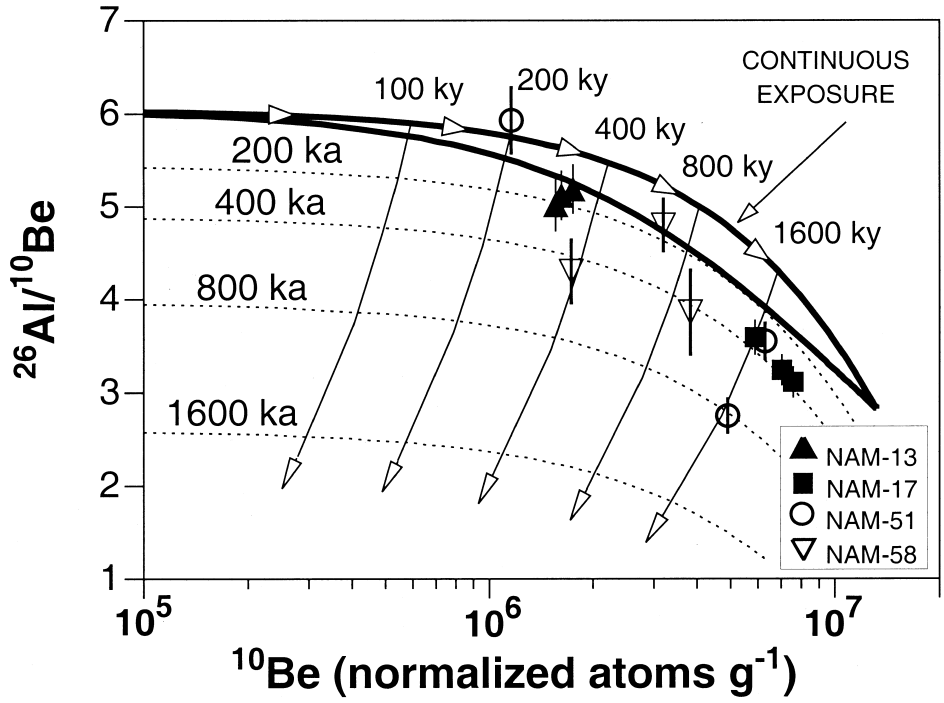

Fig. 14. Two isotope plot for 12 clast samples collected from 4 surfaces in Namibia, including exposure and burial isochrons, shows that clasts have a variety of histories. Seven clasts have histories that include significant burial after or during exposure to cosmic rays because they plot more than one sigma below the envelope consistent with steady erosion and continuous surface exposure using production rates of Nishiizumi and others (1989). Minimum initial surface exposure times indicted in ky. Minimum burial times indicated in ka. Only samples from surface NAM-13, collected within the escarpment zone and shown by upright triangles, are consistent with steady erosion without complex exposure and burial history. For additional explanation of the two-isotope diagram in terms of total sample history see Bierman and others (1999).

The three clasts collected from site NAM-13, a surface within the escarpment zone, are strikingly different in their cosmogenic nuclide signature than clasts collected elsewhere (figs. 13 and 14). As a group, the NAM-13 clasts have much more similar and far lower nuclide abundances than measured in almost all other clast samples. Only clasts collected from site NAM-13 are isotopically consistent with a model of steady erosion at rates near 2 m my^{-1} with little or no burial. This isotopic conclusion makes sense; drainages near NAM-13 are incised several to 10 m implying that the geomorphic surface, affected by the presence of the escarpment nearby, is actively eroding. Such erosion limits clast residence time and continually exposes new clasts from below.

DISCUSSION

Cosmogenic nuclide data provide a window into the past behavior of the Namibian landscape. Quantitative estimates of denudation rates allow us to consider how rapidly and in what way landscape elements have changed over time; specifically, by knowing how quickly different parts of the landscape are eroding, we can consider the concept of steady state in terms of landform shape and rates of mass removal over time and space.

Tempo and Distribution of Erosion

Cosmogenic nuclide data indicate that the Namibian landscape, while relatively stable (compare other erosion rate data in Saunders and Young, 1983), is dynamic (fig. 15). Slow, and in some cases differential, erosion is removing mass from outcrops and drainage basins at rates between 1 and 16 m my^{-1}. In general, bare rock outcrops, standing above the plains as hills and inselbergs, have the highest nuclide abundances and thus the lowest model erosion rates. Cosmogenically estimated rates of mass removal are similar to those estimated by fission track (2-14 m my^{-1}, Cockburn and others, 2000) and by the unroofing of Karoo rocks and dated kimberlites in South Africa (3.5 and 10 m my^{-1}, respectively, Partridge and Maud, 1987).

The inability to detect climate or lithology-dependent differences (fig. 9) in average bare rock erosion rates (excepting the above-average stability of massive quartz veins and the Gamsburg quartzite sampled by Cockburn and others, 2000) may be the result of several factors. Near the coast, where precipitation is least, coastal fogs are common and deposit many centimeters of liquid each year, raising effective moisture levels (Jacobsen, Jacobsen, and Seely, 1995). Also, deposition of salt, and thus probably salt-induced weathering, increase near the coast. The rapid drainage of rainwater from bare rock outcrops is sufficient to create microclimates of effectively equal aridity across the >5X rainfall gradient from which our samples were collected. This finding is in contrast to the positive linear relationship between minimum measured bedrock erosion rates and mean annual precipitation for similar samples from more humid

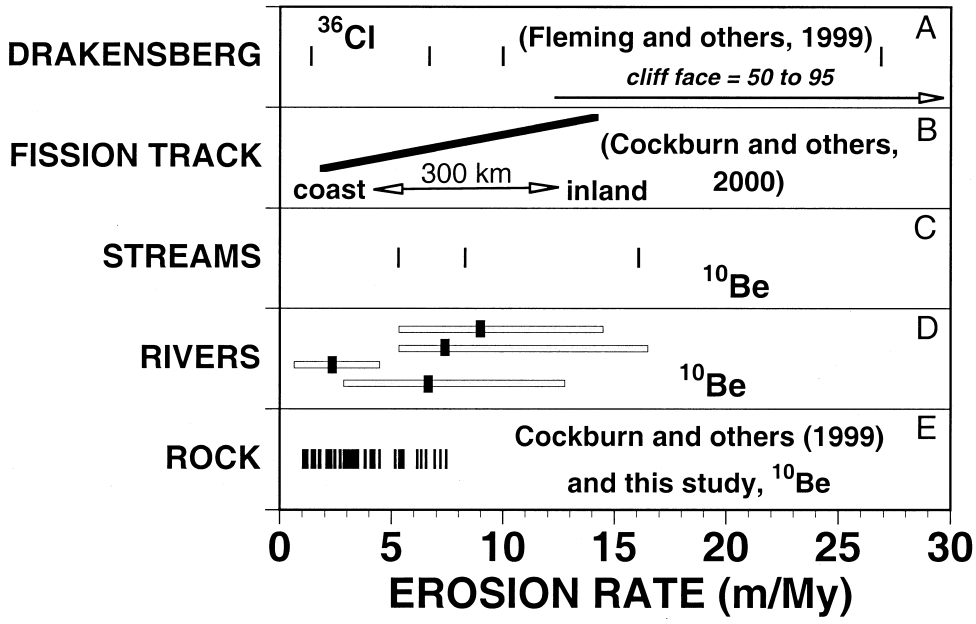

Fig. 15. Summary diagram of erosion rates in southern Africa determined over different time frames and using different methods. (A) ^{36}Cl measurements on Drakensberg Escarpment, South Africa (Fleming and others, 1999). (B) Thermal modeling of fission track measurements, central Namibia (Cockburn and others, 2000). (C) Basin-scale model erosion rates determined from ^{10}Be abundance of stream sediments (this study). (D) Basin-scale model erosion rates determined from ^{10}Be abundance of river sediments (this study). Black bar is value calculated from weighted average nuclide production rate for basin. Gray box is range of possible erosion rates consistent with nuclide abundance and range of elevations in drainage basin (table 4). (E) Bare bedrock model erosion rates; vertical bars represent range of erosion rates at 52 points on the Namibian landscape (data from this study, n=47, and Cockburn, Seidl, and Summerfield, 1999, n = 5).

regions (Bierman, 1995a, b). For example, in Georgia, where over a meter of precipitation falls yearly, granite and gneiss erode at rates exceeding 7 m my^{-1} (Bierman, 1993, 1995a).

Implications for Escarpment Retreat

Nuclide abundances we measured in sediments suggest that the escarpment zone, where local relief is significant, is eroding more quickly than either the highlands or the coastal plain supporting the recent work of Fleming and others (1999) and Cockburn and others (2000). However, even though the highest erosion rate we measured in Namibia using cosmogenic nuclides was from sediment shed by the escarpment, the rate of mass loss implied by this measurement (20 tons $km^{-2}\,yr^{-1}$, NAM-9) is nearly two orders of magnitude less than the average mass loss rate (1350 tons $km^{-2}\,yr^{-1}$) implied by uniform parallel retreat since continental breakup 130 my. Similarly, fission track data do not show rapid unroofing near the escarpment as would be the case if large amounts of mass were being removed by rapid retreat. Together, cosmogenic, off shore sediment loading (Ward and Corbett, 1990), and fission track data (Cockburn and others, 2000; van der Beek and others, 1998) can be used to argue against the validity of King's hypothesis for steady retreat of the Namibian Escarpment at rates approaching 1 km my^{-1}. The conclusion of slow if any retreat of the Namibian escarpment is similar to that of Summerfield and others (1997) who found that the Drakensberg escarpment of southern Africa is currently retreating only slowly and that coastal zone denudation there also occurred rapidly after initial continental breakup, 130 Ma. Escarpments of the southern African continent appear to be stable, slowly eroding landscape features.

Landscape Behavior

Comparing outcrop data (point erosion rate estimates) to limited sediment data from small drainage basins (basin-scale sediment generation rate estimates) indicates that outcrops are more resistant to erosion than drainage basins as a whole, a finding repeatedly reported by others (Bierman, 1994; Clapp and others, 2000, 2001; Clapp, Bierman, and Caffee, accepted; Small, Anderson, and Hancock, 1999; Heimsath and others, 1999, 2000). This difference suggests that relief may grow over time until inselbergs, with relatively stable tops, are consumed by erosion from their margins (Twidale and Bourne, 1975; Bierman and others, 1995). A similar pattern of differential erosion is consistent with cosmogenic data from the Gamsburg where a flat-lying, resistant quartzite cap protects the summit as the steep granitic sides erode 4 to 50 times more quickly (Cockburn and others, 2000).

In contrast, samples from the extremely flat-lying and extensive gravel surfaces consolidated by pedogenic processes (specifically the deposition of calcrete and gypcrete) have the highest cosmogenic nuclide abundance. Several surface clasts have near-surface exposure histories approaching 3 my; such extreme stability has been found only in the hyperarid Atacama Desert (Nishiizumi and others, 1998) and parts of Antarctica where liquid water is usually absent (Nishiizumi and others, 1991). Presumably such extraordinary stability is the result of extended dry conditions, the lack of well developed drainage networks on these surfaces, and low surface gradients. It is possible that erosion-resistant clasts float on slowly deflating surfaces (Wells and others, 1995) increasing their dosing over time as the surface lowers beneath them.

Steady State Behavior?

Our basin-integrating cosmogenic sediment data, when considered along with fission track thermal histories (Cockburn and others, 2000), indicate that regional denudation rates are similar over two very different time scales. Fission tracks suggest that long-term (0-36 my) average erosion rates near the coast have been several meters

per million years rising to between 8 and 15 m my^{-1} in the highlands. These rates are consistent with the basin-scale rates we measure (table 4) in streams (5-16 m my^{-1}) and rivers (3-9 m my^{-1}). Together, the data suggesting that the entire Namibian margin has been eroding at similar rates over the past 36 my implying steady-state, in terms of erosion rates, since the mid-Tertiary.

We find no significant difference between bare rock erosion rates above and below the Namibian Escarpment, implying that exposed coarse crystalline rocks in the highlands and on the coastal plain are lowering at similar rates. Thus, cosmogenic data support the fission-track and sediment-volume based conclusion, that coastal plain lowering occurred rapidly post-rifting and that differential erosion of the coastal plain is no longer occurring (Ward and Corbett, 1990; Brown and others 2000; Cockburn and others, 2000). Because we cannot detect any spatial patterning of erosion rates and because the erosion rates we measured are generally very slow, the Namibian landscape is approaching a geomorphic steady state where its overall shape changes only slowly, if at all, over time.

Cosmogenic data indicate that the Namibian landscape as a whole is eroding so slowly that large landforms, the overall topography, and the geomorphic appearance change little over 10^5 to 10^6 yr. The isotopic ratio data ($^{26}Al/^{10}Be$) for our bedrock samples are consistent with slow, steady erosion of the bare rock outcrops; we find little evidence for episodic burial nor for episodic loss of thick sheets of rock as suggested by Cockburn, Seidl, and Summerfield (1999) for several of their 6 samples. This finding of landscape stability is buttressed by isotopic data from just north of the Namib Sand Sea (NAM-23 to -26), which suggest that over the past $10^5 - 10^6$ yrs, the Kuiseb River has prevented sand from migrating northward and burying granite outcrops. Similarly, the lack of burial in samples from the base of an inselberg near Vogelfederberg argues for extreme stability in terms of the location of regolith and aeolian cover.

Thus, we conclude that Namibian landscape approaches steady-state in three ways. First, it erodes so slowly that the landforms appear steady and little changing over geomorphic time scales of 10^4 to 10^5 yr. Second, the spatial similarity of rock and basin-scale erosion rates below and above the escarpment precludes differential erosion that would change overall landscape morphology unidirectionally. Third, the steadiness of erosion rates over time is suggested by the coincidence of cosmogenic and fission-track based rates of rock removal.

ACKNOWLEDGMENTS

Support for field and laboratory work was provided by grant 5858-97 to Bierman from the National Geographic Society. Additional support for analysis of sediment samples provided by NSF Hydrologic Sciences grant EAR-9628559 to Bierman. Partial support for this work provided by Department of Energy under contract W7405-ENG-48 to Caffee. We thank S. Neis, B. Copans, and J. Larsen for sample processing and analysis, C. Massey for field assistance, J. Southon for AMS assistance, and K. Nichols, R. Brown, F. Pazzaglia, A. Heimsath, and an anonymous reviewer for extensive comments on and assistance with the manuscript.

References

Bierman, P. R., ms, 1993, Cosmogenic isotopes and the evolution of granitic landforms: Ph.D. thesis, University of Washington, Seattle, 273 p.

——— 1994, Using in situ cosmogenic isotopes to estimate rates of landscape evolution: A review from the geomorphic perspective: Journal of Geophysical Research, v. 99, p. 13885–13896.

——— 1995a, How fast do rocks erode? New answers from atom counting: Geological Society of America Abstracts with Programs, v. 27, p. A-44.

——— 1995b, A new method of estimating basin scale erosion rates — measurement of in situ produced ^{10}Be and ^{26}Al in sediments: EOS, v. 76, p. S143.

Bierman, P. R., Gillespie, A., Caffee, M., and Elmore, D., 1995, Estimating erosion rates and exposure ages with ^{36}Cl produced by neutron activation: Geochemica et Cosmochemica Acta, v. 59, p. 3779–3798.

Bierman, P. R., Marsella, K. A., Davis, P. T., Patterson, C., and Caffee, M., 1999, Mid-Pleistocene cosmogenic minimum-age limits for pre-Wisconsinan glacial surfaces in southwestern Minnesota and southern Baffin Island — a multiple nuclide approach: Geomorphology, v. 27, p. 25–40.

Bierman, P. R., and Steig, E., 1996, Estimating rates of denudation and sediment transport using cosmogenic isotope abundances in sediment: Earth Surface Processes and Landforms, v. 21, p. 125–139.

Bierman, P. R., and Turner, J., 1995, ^{10}Be and ^{26}Al evidence for exceptionally low rates of Australian bedrock erosion and the likely existence of pre-Pleistocene landscapes: Quaternary Research, v. 44, p. 378–382.

Brown, E. T., Bourles, D. L., Colin, F., Raisbeck, G. M., Yiou, F., and Desgarceaux, S., 1995a, Evidence for muon-induced production of ^{10}Be in near surface rocks from the Congo: Geophysical Research Letters, v. 22, p. 703–706.

Brown, E. T., Stallard, R. F., Larsen, M. C., Raisbeck, G. M., and Yiou, F., 1995b, Denudation rates determined from the accumulation of in situ-produced ^{10}Be in the Luquillo Experimental Forest, Puerto Rico: Earth and Planetary Science Letters, v. 129, p. 193–202.

Brown, R., Gallagher, K., Gleadow, A. J. W., and Summerfield, M. A., 2000, Morphotectonic evolution of the South Atlantic margins of Africa and South America, *in* Summerfield, M. A., editor, Geomorphology and Global Tectonics, Chichester, Wiley, p. 255–281.

Cerling, T. E., and Craig, H., 1994, Geomorphology and in-situ cosmogenic isotopes: Annual Review of Earth and Planetary Science, v. 22, p. 273–317.

Clapp, E. M., Bierman, P. R., and Caffee, M., in press, Using ^{10}Be and ^{26}Al to determine sediment generation rates and identify sediment source in an arid region drainage basin: Geomorphology.

Clapp, E., Bierman, P. R., Pavich, M., and Caffee, M., 2001, Rates of sediment supply to arroyos from uplands determined using in situ produced cosmogenic ^{10}Be and ^{26}Al in sediments: Quaternary Research, v. 55, n. 2. p. 235–245.

Clapp, E. M., Bierman, P. R., Schick, A. P., Lekach, J., Enzel, Y., and Caffee, M., 2000, Differing rates of sediment production and sediment yield: Geology, 28, p. 995–998.

Clark, D., Bierman, P. R., and Larsen, P., 1995, Improving in situ cosmogenic chronometers: Quaternary Research, v. 44, p. 366–376.

Cockburn, H. A. P., Brown, R. W., Summerfield, M. A., and Seidl, M. A., 2000, Quantifying passive margin denudation and landscape development using a combined fission-track thermochronology and cosmogenic isotope approach: Earth and Planetary Science Letters, v. 79, no. 3–4 , p. 429–435

Cockburn, H. A. P., Seidl, M. A., and Summerfield, M. A., 1999, Quantifying denudation rates on inselbergs in the central Namib Desert using in situ-produced cosmogenic ^{10}Be and ^{26}Al: Geology, v. 27, p. 399–402.

Davis, R., and Schaeffer, O. A., 1955, Chlorine-36 in nature: Annals of the New York Academy of Science, v. 62, p. 105–122.

Desilets, D. and Zreda, M., 2000, Scaling production rates of terrestrial cosmogenic nuclides for altitude and geomagnetic effects, Geological Society of America Abstracts with Programs, 31 (7), p. A-400.

Dunai, T., 2000, Scaling factors for production rates of in situ produced cosmogenic nuclides: a critical reevaluation: Earth and Planetary Science Letters, v. 176, p. 157–169.

Elmore, D., and Phillips, F., 1987, Accelerator mass spectrometry for measurement of long-lived radioisotopes: Science, v. 236, p. 543–550.

Finkel, R., and Suter, M., 1993, AMS in the Earth Sciences: Technique and applications: Advances in Analytical Geochemistry, v. 1, p. 1–114.

Fleming, A., Summerfield, M. A., Stone, J. O., Fifield, L. K., and Cresswell, R. G., 1999, Denudation for the southern Drakensberg escarpment, SE Africa derived from in-situ-produced cosmogenic ^{36}Cl: Initial results: Geological Society (London) Journal, v. 156, p. 209–212.

Gallagher, K., and Brown, R., 1997, The onshore record of passive margin evolution: Journal of the Geological Society (London) v. 154, p. 451–457.

——— 1999, The Mesozoic denudation history of the Atlantic margins of southern Africa and southeast Brazil and the relationship to offshore sedimentation, *in* Cameron, N. R., Bate, R. H., and Clure, V. S., editors, The Oil and Gas Habits of the South Atlantic: Geological Society (London) Special Publications, p. 41–53.

Gilchrist, A. R., Kooi, H., and Beaumont, C., 1994, Post Gondwana geomorphic evolution of southwestern Africa: implications for the controls on landscape development from observations and numerical experiments: Journal of Geophysical Research, v. 99, p. 739–742.

Gilchrist, A. R., and Summerfield, M. A., 1990, Tectonic models of passive margin evolution and their implications for theories of long-term landscape development, *in* Kirkby, M. J., editors, Process Models and Theoretical Geomorphology: Chichester, Wiley. p. 55–84.

Gillespie, A. R., and Bierman, P. R., 1995, Precision of terrestrial exposure ages and erosion rates from analysis of in-situ produced cosmogenic isotopes: Journal of Geophysical Research, v. 100, p. 24,637–24,649.

Gosse, J. C., Klein, J., Evenson, E. B., Lawn, B., and Middleton, R., 1995. Beryllium-10 dating of the duration and retreat of the last Pinedale glacial sequence. Science, v. 268, p. 329–1333.

Goudie, A., 1972, Climate, weathering, crust formation, dunes and fluvial features of the central Namib Desert near Gobabeb, Southwest Africa: Madoqua, series II, v. 1, n. 54–62, p. 15–31.

Granger, D. E., Kirchner, J. W., and Finkel, R., 1996, Spatially averaged long-term erosion rates measured from in-situ produced cosmogenic nuclides in alluvial sediment: Journal of Geology, v. 104, p. 249–257.

——— 1997, Quaternary downcutting rate of the New River, Virginia, measured from differential decay of cosmogenic ^{10}Be and ^{26}Al in cave-deposited alluvium: Geology, v. 25, p. 107–110.

Granger, D. E., and Smith, A. L., 2000, Dating buried sediments using radioactive decay and muogenic production of ^{26}Al and ^{10}Be, Nuclear Instruments and Methods in Physics Research B, v. 172, p. 822–826.
Hack, J. T., 1960, Interpretation of erosional topography in humid temperate regions: American Journal of Science, v. 258A, p. 80–97.
Heimsath, A. M., Chappell, J., Dietrich, W. E., Nishiizumi, K., and Finkel, R. C., 2000, Soil production on a retreating escarpment in southeastern Australia, Geology, v. 28, p. 787–790.
Heimsath, A. M., Dietrich, W. E., Nishiizumi, K., and Finkel, R. C., 1999, Cosmogenic nuclides, topography, and the spatial variation of soil depth: Geomorphology, v. 27, p. 151–172.
Heine, K., 1985, Late Quaternary development of the Kuiseb River valley and adjacent areas, central Namib desert, south west Africa/Namibia and paleoclimatic implications: Zeitschrift fur Gletscherkunde und Glazialgeologie, v. 21, p.151–157.
Jacobsen, P. J., Jacobsen, K. M., and Seely, M. K., 1995, Ephemeral rivers and their catchments: Windhoek, Desert Research Foundation of Namibia, 160 p.
King, L. C., 1953, Canons of landscape evolution: Geological Society of America Bulletin, v. 64, p. 721–752.
——— 1957, The uniformatarian nature of hillslopes: Edinborough Geological Society Transactions, v. 17, p. 81–104.
——— 1966, The origin of bornhardts: Zeitschrift fur Geomorphologie, v. 10, p. 97–98.
——— 1967, The morphology of the Earth: Edinborough, Oliver and Boyd, 726 p.
Klein, J., Giegengack, R., Middleton, R., Sharma, P., Underwood, J. R., and Weeks, R. A., 1986, Revealing histories of exposure using in situ produced ^{10}Be and ^{26}Al in Libyan desert glass: Radiocarbon, v. 28, p. 547–555.
Kohl, C. P., and Nishiizumi, K., 1992, Chemical isolation of quartz for measurement of *in-situ* -produced cosmogenic nuclides: Geochimica et Cosmochimica Acta, v. 56, p. 3583–3587.
Kooi, H., and Beaumont, C., 1994, Escarpment evolution on high-elevation rifted margins: Insights derived from a surface processes model that combines diffusion, advection, and reaction: Journal of Geophysical Research, v. 99, p. 12,191–12,209.
Lal, D., 1988, In situ-produced cosmogenic isotopes in terrestrial rocks: Annual Reviews of Earth and Planetary Science, v. 16, p. 355–388.
——— 1991, Cosmic ray labeling of erosion surfaces: *In situ* production rates and erosion models: Earth and Planetary Science Letters, v. 104, p. 424–439.
Lal, D., and Peters, B., 1967, Cosmic ray produced radioactivity on the earth, *in* Sitte, K., editor, Handbuch der Physik, New York, Springer-Verlag, p. 551–612.
Miller, R., 1983, Evolution of the Damara Orogen: Geological Society of South Africa Special Paper, v. 11.
Miller, R., and Schalk, K. E. L., 1980, Geologic map of Namibia: Geological Survey of Namibia.
Nichols, K. K., Bierman, P. R., Hooke, R. and Caffee, M., in press, Understanding desert Piedmonts using in situ produced ^{10}Be and ^{26}Al : Geomorphology.
Nishiizumi, K., Finkel, R., Brimhall, G., Mote, T., Mueller, G., and Tidy, E., 1998, Ancient exposure ages of alluvial fan surfaces compared with incised stream beds and bedrock in the Atacama Desert of north Chile: Geological Society of America Abstracts with programs, v. 30, p. A-298.
Nishiizumi, K., Kohl, C. P., Arnold, J. R., Klein, J., Fink, D., and Middleton, R., 1991, Cosmic ray produced ^{10}Be and ^{26}Al in Antarctic rocks: exposure and erosion history: Earth and Planetary Science Letters, v. 104, p. 440–454.
Nishiizumi, K., Lal, D., Klein, J., Middleton, R., and Arnold, J. R., 1986, Production of ^{10}Be and ^{26}Al by cosmic rays in terrestrial quartz *in situ* and implications for erosion rates: Nature, v. 319, p. 134–136.
Nishiizumi, K., Winterer, E. L., Kohl, C. P., Klein, J., Middleton, R., Lal, D., and Arnold, J. R., 1989, Cosmic ray production rates of ^{10}Be and ^{26}Al in quartz from glacially polished rocks: Journal of Geophysical Research, v. 94, p. 17907–17915.
Oberlander, T. M., 1972, Morphogenesis of granitic boulder slopes in the Mojave desert, California: Journal of Geology, v. 80, n. 1, p. 1–20.
Ollier, C. D., 1977, Outline geological and geomorphological history of the central Namib Desert, Madoqua, v. 10, n. 3, p. 213–214.
——— 1978, Inselbergs of the Namib Desert process and history: Zeitschrift fur Geomorphologie, Supplement, v. 31, p. 161–176.
Partridge, T. C. and Maud, R. R., 1987, Geomorphic evolution of Southern Africa since the Mesozoic: Transactions of the Geological Society of South Africa, v. 90, no. 2, p.179–208.
Penck, W., 1924, Die morphologeist analyse ein Kapital der physikalische geologie: Stuttgart, Engelhorn.
Saunders, I., and Young, A., 1983, Rates of surface processes on slopes, slope retreat, and denudation: Earth Surface Processes and Landforms, v. 8, p. 473–501.
Seidl, M. A., Weissle, J. K., and Pratson, L. F., 1996, The kinematics and pattern of escarpment retreat across the rifted continental margin of SE Australia: Basin Research, v. 8, p. 301–316.
Selby, M. J., 1977, Bornhardts of the Namib desert: Zeitschrift fur Geomorphologie, v. 21, p. 1–13.
——— 1982a, Form and origin of some bornhardts of the Namib Desert: Zeitschrift fur Geomorphologie, v. 26, p. 1–15.
——— 1982b, Rock mass strength and the form of some inselbergs in the central Namib Desert: Earth Surface Processes and Landforms, v. 7, p. 489–497.
Selby, M. J., Hendy, C. H., and Seely, M. K., 1979, A late Quaternary lake in the central Namib desert, southern Africa, and some implications: Paleogeography, Paleoclimatology, Paleoecology, v. 26, p. 37–41.
Small, E. E., Anderson, R. S., and Hancock, G. S., 1999, Estimates of the rate of regolith production using ^{10}Be and ^{26}Al from an alpine hillslope: Geomorphology, v. 27, p. 131–150.

Stone, J. O., Ballantyne, C. K., and Fifield, L. K., 1998, Exposure dating and validation of periglacial weathering limits, northwest Scotland: Geology, v. 26, p. 587–590.
Stone, J. O., Lambeck, K., Fifield, L. K., Evans, J. M. and Cresswell, R. G., 1996, A late glacial age for the main rock platform, western Scotland: Geology, v. 24, p. 707–710.
Summerfield, M. A., Brown, R. W., Van Der Beek, P., and Braun, J., 1997, Drainage divides, denudation, and the morphotectonic evolution of high-elevation passive margins: Geological Society of America, Abstracts with Programs, v. 29, p. 476.
Thomas, M. F., 1978, The study of inselbergs: Zeitschrift fur Geomorphologie, supplement, v. 31, p. 111–137.
Tucker, R. and Slingerland, 1994, Erosional dynamics, flexural isostasy, and long-lived escarpments: A numerical modeling study: Journal of Geophysical Research, v. 99, p. 12,229–12,243.
Twidale, C. R., 1978, Bornhardts: Zeitschrift fur Geomorphologie, supplement, v. 31, p. 111–137.
Twidale, C. R., and Bourne, J. A., 1975, Episodic exposure of inselbergs: Geological Society of America Bulletin, v. 86, p. 1473–1481.
van der Beek, P., Braun, J., Summerfield, M., and Brown, R., 1998, Morphotectonic evolution of rifted margins: not just flank uplift and escarpment retreat: Annales Geophysicae, v. 16, p. 75.
Ward, J. D., 1987, The Cenozoic succession in the Kuiseb Valley, central Namib Desert: Geological Survey of Namibia Memoir, v. 9, p. 124.
Ward, J. D. and Corbett, I., 1990, Towards an age for the Namib, in: Seely, M.K., ed., Namib ecology: 25 years of Namib research: Transvaal Museum Monograph 7, Pretoria, p. 17–26.
Wells, S. G., McFadden, L. D., Poths, J., and Olinger, C. T., 1995, Cosmogenic ^{3}He surface exposure dating of stone pavements: implications for landscape evolution in deserts: Geology, v. 23, p. 613–616.